

# Signatures of topology in generic transport measurements for Rarita-Schwinger-Weyl semimetals

Ipsita Mandal<sup>1,\*</sup>, Shreya Saha<sup>1</sup>, and Rahul Ghosh<sup>2</sup>

<sup>1</sup>*Department of Physics, Shiv Nadar Institution of Eminence (SNIoE),  
Gautam Buddha Nagar, Uttar Pradesh 201314, India*

<sup>2</sup>*Department of Physical Sciences, Indian Institute of Science  
Education and Research Berhampur, Berhampur, Odisha 760010, India*

We investigate how the signatures of the topological properties of the bandstructures for nodal-point semimetals are embedded in the response coefficients, arising in two distinct experimental set-ups, by taking the Rarita-Schwinger-Weyl (RSW) semimetal as an example. The first scenario involves the computation of third-rank tensors representing second-order response coefficients, relating the charge/thermal current densities to the combined effects of the gradient of the chemical potential and an external electric field/temperature gradient. On the premises that internode scatterings can be ignored, the relaxation-time approximation leads to a quantized value for the non-vanishing components of each of these nonlinear response tensors, characterizing a single untilted RSW node. Furthermore, the final expressions turn out to be insensitive to the specific values of the chemical potential and the temperature. The second scenario involves computing the magneto-electric conductivity under the action of collinear electric ( $\mathbf{E}$ ) and magnetic ( $\mathbf{B}$ ) fields, representing a planar Hall set-up. In particular, our focus is in bringing out the dependence of the linear-in- $|\mathbf{B}|$  parts of the conductivity tensor on the intrinsic topological properties of the bandstructure, which are nonvanishing only in the presence of a nonzero tilt in the energy spectrum.

## I. INTRODUCTION

Three-dimensional (3d) topological semimetals [1–4] form the gapless cousins of the topological insulators (for which a gap-opening implying a topological phase transition), possessing a gapless spectrum. Weyl semimetals (WSMs) exemplify such topological phases, forming an intermediate state in the transition from metals to insulators, in which the conduction and the valence bands touch only at discrete points. This leads to the emergence of zero band-gap and singular points in the Brillouin zone (BZ), known as nodal points, where the density-of-states vanish exactly. The nodal are topologically stable as they cannot be fully gapped out by perturbations that are small (in magnitude) and local in momentum space, such that the bulk gap remains intact sufficiently away from the band-crossing points. The stability of the nodal points and, consequently, the gaplessness of the semimetallic phases are ensured by the fact these points act as the sources/sinks of topological charges (leading to the noting of defective or singular points). Although the topological charges are determined by the electronic bandstructure of the material, often they are not directly measurable. However, two experimentally-accessible and exploitable properties that appear are:

1. Quantized response in various transport measurements that depend on the intrinsic Berry curvature (BC) of the bandstructures. Some examples include circular dichroism [5, 6], circular photogalvanic effect [7–10], and Magnus Hall effect [11–13].
2. Fermi arcs surface states at the two-dimensional (2d) surface BZ [3].

Although not in the form of a quantized response, the signatures of BC are very much present in numerous other transport properties, such as intrinsic anomalous Hall effect [14–16], planar Hall effects [17–36], magneto-optical conductivity with strong (quantizing) magnetic field [37–39], transmission of quasiparticles across barriers/wells of electric potential [40–44].

In the WSMs [1, 2], we encounter twofold band-crossing singularities, with each band having an isotropic linear-in-momentum dispersion in the vicinity of the nodal point. The 230 space groups in nonrelativistic condensed matter physics allows the possibility of richer bandstructures in the form symmetry-protected multifold band-crossings [45]. The simplest case is the one where each band exhibits an isotropic linear-in-momentum dispersion, akin to the WSMs. In general, the effective low-energy Hamiltonian of such a system is captured by  $\sim \mathbf{k} \cdot \mathcal{S}$ , where  $\mathcal{S}$  is the vector operator comprising the three components of the angular momentum in the spin- $\varsigma$  representation of the SO(3) group. This stems from the  $(2\varsigma + 1)$  bands touching at the nodal point, resulting in the itinerant electronic degrees of freedom represented by quasiparticles with pseudospin quantum numbers equalling  $\varsigma$ . The terminology of “pseudospin” is used in order to clearly demarcate it as a quantum number distinct from the relativistic spin of an electron. While WSMs feature  $\varsigma = 1/2$ , the poster child for multifold cases is the Rarita-Schwinger-Weyl (RSW) semimetal [5, 13, 36, 44–53], having pseudospin-3/2 (i.e., fourfold band-crossings). This nomenclature is inspired by the fact that in the branch of theoretical high-energy physics, the

---

\* ipsita.mandal@snu.edu.in

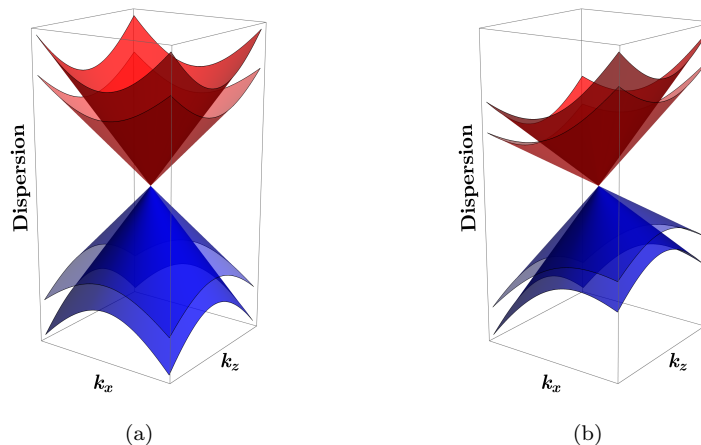


FIG. 1. Schematics of the dispersions of the four bands at a single RSW node: Subfigures (a) and (b) represent an untitled node (i.e.,  $\eta = 0$ ) and a tilted node (with  $0 < |\eta| < 1$ ), respectively.

Rarita-Schwinger (RS) equation describes the field equation of elementary particles with the relativistic spin of  $3/2$ , which naturally arise in supergravity models [54]. Albeit, these higher-spin fermionic particles appear neither in the standard model of particle physics, nor has been detected experimentally. The RSW semimetals thus present a nonrelativistic analogue of the elusive RS fermions in the context of solid-state systems.

Let us now elaborate on the origins of the BC and the quantized-response phenomena in widely different experimental settings. The *topological* properties of a crystalline bandstructure are inferred by treating the BZ as a closed manifold. A nodal-point semimetal is endowed with a nontrivial topology when the nodes demarcate point-like topological defects, mathematically quantified as the locations of the BC monopoles [4, 55]. The charge of a BC monopole, therefore, is a topological charge, whose sign assigns a chirality  $\chi$  to the node, with  $\chi = +1$  and  $\chi = -1$  labelling the so-called *right-moving* and *left-moving chiral* quasiparticles, respectively. Here, we will adopt the widely-used convention of assigning  $\chi = 1$  to the bands with negative energy (with respect to the band-crossing point). The physical picture thus represents that a positively-charged (negatively-charged) monopole acts as a source (sink) for the BC flux lines. Using all the above definitions, we find that the monopole charge of a specific band is computed by employing the familiar Gauss's law, where we integrate the BC flux over a closed 2d surface enclosing the point-defect. If we project on to the space of a pair of bands with the same magnitude of the pseudospin magnetic quantum numbers, we get a two-level system — the Chern number ( $\mathcal{C}$ ) represents a wrapping number of the map from the 2d closed surface (topologically equivalent to  $S^2$ ) to the Bloch sphere ( $S^2$ ), given by the elements of the second homotopy group  $\Pi_2(S^2) = \mathbb{Z}$ . Thus the monopole charges are equivalent to the Chern numbers, when interpreted as the wrapping numbers of the defects. The monopole charges points always appear in pairs, with each pair having the values  $\pm\mathcal{C}$ , thus satisfying the Nielsen-Ninomiya theorem [56]. Our aim in this paper is to unravel some transport coefficients for an RSW node which show a quantized nature, being proportional to  $\mathcal{C}$ , thus revealing the nature of the underlying topology. In this context, it is necessary to point out that the four bands at a single RSW node have Chern numbers  $\pm 1$  and  $\pm 3$ , which sum up to a net monopole charge of magnitude 4 (considering either the two upper or the two lower bands). Therefore, while a WSM-node harbours a Berry monopole charge of magnitude unity, an RSW hosts a net monopole charge of a higher-integer value. In this paper, we will show how these higher values of charges may show up as quantized response in various experimental set-ups. In fact, the signatures of the existence of RSW quasiparticles are believed to be reflected by the large values of the topological charges detected in a range of materials, such as CoSi [57], RhSi [58], AlPt [59], and PdBiSe [60].

In this paper, we consider the quantization associated with two distinct experimental set-ups:

1. Nonlinear transport under the effect of an external electric field (and/or temperature gradient) and the gradient of the chemical potential, constituting a response of electrochemical (or thermochemical) nature [61]. Here, we dub the associated electrical and thermal conductivity tensors as the electrochemical response (ECR) and thermochemical response (TCR), respectively. For a single untitled node of WSM, the ECR has been shown to take quantized values for temperature  $T$  equalling zero [61]. However, there were various shortcomings in their steps to derive the form of the response, which we will clarify in the course of our computations. Moreover, we will show the quantized nature of both the ECR and the TCR considering a *generic temperature*<sup>1</sup> for the fourfold nodal point of the RSW, which is a multiband generalization of the WSM case.

<sup>1</sup> Albeit with the constraint  $T \ll \mu$  (while using natural units), so that we are in the low-energy limit where the effective continuum model for the node is valid. Since  $\mu$  ranges around 0.01-0.1 eV [50], we must have  $T \lesssim 10^{-3}$  eV. For example, recent experiments [62] probe response setting the temperature ranges of the order of  $8.617 \times 10^{-5} - 8.617 \times 10^{-3}$  eV, which is equivalent to  $\sim 1 - 100$  K (in SI units).

2. Components of the magnetoelectric conductivity under the action of electric ( $\mathbf{E}$ ) and magnetic ( $\mathbf{B}$ ) fields, applied parallel to each other, constituting a planar Hall set-up. Here, we will demonstrate the quantized nature of the linear-in- $B$  parts of the linear-response tensor, arising from the four bands of an RSW node.

The paper is organized as follows. In Sec. II, we outline the form of the low-energy effective Hamiltonian in the vicinity of an RSW node and, also, show the expressions for various topological quantities. While Sec. III deals with the nonlinear response coefficients dubbed as ECR and TCR, Sec. IV focusses on the linear response associated with the magnetoelectric conductivity. In the end, we wrap up with a summary and outlook in Sec. V. In Appendix A, the details of the derivations of the response tensors, applying the semiclassical Boltzmann formalism, are provided. The remaining appendices are devoted to elaborating on some of the details of the intermediate steps, necessary to derive the final expressions shown in the main text. In all our expressions, we resort to using the natural units, which implies that the reduced Planck's constant ( $\hbar$ ), the speed of light ( $c$ ), and the Boltzmann constant ( $k_B$ ) are each set to unity.

## II. MODEL

With the help of group-theoretic symmetry analysis and first principles calculations, it has been shown that seven space groups may host fourfold band-crossing points [45] at high-symmetry points of the BZ. Nearly 40 candidate materials have also been identified that can host the resulting RSW quasiparticles. Ref. [63] has tabulated the multifold degeneracies in the 65 chiral space groups characterizing the chiral crystals, which are the ones with only orientation-preserving symmetries. A chiral fourfold band-crossing can be realized in the space groups (1) 195–198 and 207–214 at the  $\Gamma$ -point; (2) 207 and 208 at the  $R$ -point; and (3) 211 and 214 at the  $H$ -point, in the presence of spin-orbit coupling. These fourfold degeneracies exhibit a BC texture that is homotopic to that of a spin-3/2 moment in a magnetic field. The RSW semimetal, with the effective Hamiltonian possessing a full SU(2) invariance (i.e., a full rotational invariance). It has been shown [64] that chiral topological metals belonging to the SrGePt family (e.g., SrSiPd, BaSiPd, CaSiPt, SrSiPt, BaSiPt, and BaGePt), characterized by the space group 198, host RSW quasiparticles, sixfold excitations (two copies of pseudospin-1 fermions), as well as Weyl points in their bandstructures, when spin-orbit coupling is considered. More explicitly, a fourfold-degenerate node appears at the center of the BZ (i.e., the  $\Gamma$ -point), carrying the monopole charge of +4, while a sixfold-degenerate node arises at the boundary of the BZ (i.e., the  $R$ -point) with a net monopole charge equalling  $-2 - 2 = -4$ . Here, we ignore any internode scatterings, which is justified because the energy offset between the fourfold-degenerate point (at  $\Gamma$ ) and the sixfold-degenerate point (at  $R$ ) is usually large [50, 64–66].

The usual method of linearizing the  $\mathbf{k} \cdot \mathbf{p}$  Hamiltonian about such a degeneracy point provides us with the low-energy effective continuum Hamiltonian, valid in the vicinity of the node. The explicit form of this Hamiltonian, for a single node with chirality  $\chi$ , is given by

$$\mathcal{H}(\mathbf{k}) = \eta v_0 k_z + \chi v_0 (k_x \mathcal{J}_x + k_y \mathcal{J}_y + k_z \mathcal{J}_z), \quad (1)$$

where  $\mathcal{J} = \{\mathcal{J}_x, \mathcal{J}_y, \mathcal{J}_z\}$  represents the vector operator whose three components comprise the angular momentum operators in the spin-3/2 representation of the SO(3) group. Here,  $\eta$  represents the tilt parameter, with  $|\eta| < 1$  representing the type-I phase, which is the scenario under consideration. We choose the commonly-used representation where

$$\mathcal{J}_x = \begin{pmatrix} 0 & \frac{\sqrt{3}}{2} & 0 & 0 \\ \frac{\sqrt{3}}{2} & 0 & 1 & 0 \\ 0 & 1 & 0 & \frac{\sqrt{3}}{2} \\ 0 & 0 & \frac{\sqrt{3}}{2} & 0 \end{pmatrix}, \quad \mathcal{J}_y = \begin{pmatrix} 0 & \frac{-i\sqrt{3}}{2} & 0 & 0 \\ \frac{i\sqrt{3}}{2} & 0 & -i & 0 \\ 0 & i & 0 & \frac{-i\sqrt{3}}{2} \\ 0 & 0 & \frac{i\sqrt{3}}{2} & 0 \end{pmatrix}, \quad \mathcal{J}_z = \begin{pmatrix} \frac{3}{2} & 0 & 0 & 0 \\ 0 & \frac{1}{2} & 0 & 0 \\ 0 & 0 & -\frac{1}{2} & 0 \\ 0 & 0 & 0 & -\frac{3}{2} \end{pmatrix}. \quad (2)$$

Our convention is such that the pair of conjugate nodes are separated along the  $k_z$ -direction. The energy eigenvalues are found to be

$$\varepsilon_s(k) = s v_0 k + v_0 \eta k_z, \quad s \in \left\{ \pm \frac{1}{2}, \pm \frac{3}{2} \right\}, \quad (3)$$

where  $k = \sqrt{k_x^2 + k_y^2 + k_z^2}$ . Hence, each of four bands has a linear-in-momentum dispersion (cf. Fig. 1). The signs of “+” and “-” give us the dispersion relations for the conduction and valence bands, respectively. The corresponding group velocities of the quasiparticles are given by

$$\mathbf{v}_s(\mathbf{k}) = \nabla_{\mathbf{k}} \varepsilon_s(\mathbf{k}) = \frac{s v_0 \mathbf{k}}{k} + \eta v_0 \hat{\mathbf{z}}. \quad (4)$$

### A. Properties with topological origins

A nontrivial topology of the bandstructure of the RSW semimetals gives rise to the BC and the orbital magnetic moment (OMM), using the starting expressions of [67]

$$\boldsymbol{\Omega}_s(\mathbf{k}) = i \langle \nabla_{\mathbf{k}} \psi_s(\mathbf{k}) | \times | \nabla_{\mathbf{k}} \psi_s(\mathbf{k}) \rangle \text{ and } \mathbf{m}_s(\mathbf{k}) = -\frac{e}{2} \text{Im} [\langle \nabla_{\mathbf{k}} \psi_s | \times (\mathcal{H}(\mathbf{k}) - \varepsilon_s(\mathbf{k})) | \nabla_{\mathbf{k}} \psi_s \rangle], \quad (5)$$

respectively. Here,  $|\psi_s(\mathbf{k})\rangle$  denotes the eigenfunction for the  $s^{\text{th}}$  band at the node with chirality  $\chi$ , and  $e$  denotes the magnitude of the charge of a single electron. Evaluating these expressions for the RSW node described by  $\mathcal{H}(\mathbf{k})$ , we get

$$\boldsymbol{\Omega}_s(\mathbf{k}) = -\frac{\chi s \mathbf{k}}{k^3} \text{ and } \mathbf{m}_s(\mathbf{k}) = -\frac{e \chi v_0 \mathcal{G}_s \mathbf{k}}{k^2}, \text{ with } \mathcal{G}_{\pm\frac{3}{2}} = \frac{3}{4} \text{ and } \mathcal{G}_{\pm\frac{1}{2}} = \frac{7}{4}. \quad (6)$$

Since  $\boldsymbol{\Omega}_s(\mathbf{k})$  and  $\mathbf{m}_s(\mathbf{k})$  are the intrinsic properties of the bandstructure, they depend only on the wavefunctions. Clearly, they are related as

$$\mathbf{m}_s(\mathbf{k}) = \frac{e v_0 \mathcal{G}_s k}{s} \boldsymbol{\Omega}_s(\mathbf{k}). \quad (7)$$

We observe that, unlike the BC, the OMM does not depend on the sign of the energy dispersion.

The OMM behaves exactly like the electron spin, because, on applying a magnetic field  $\mathbf{B}$ , it couples to the field through a Zeeman-like term, quantified by

$$\zeta_s(\mathbf{k}) = -\mathbf{m}_s(\mathbf{k}) \cdot \mathbf{B} = e \chi v_0 \mathcal{G}_s \frac{\mathbf{k} \cdot \mathbf{B}}{k^2}. \quad (8)$$

Therefore, we have

$$\xi_s(\mathbf{k}) = \varepsilon_s(\mathbf{k}) + \zeta_s(\mathbf{k}), \quad \mathbf{w}_s(\mathbf{k}) = \mathbf{v}_s(\mathbf{k}) + \mathbf{u}_s(\mathbf{k}), \quad \mathbf{u}_s(\mathbf{k}) = \nabla_{\mathbf{k}} \zeta_s(\mathbf{k}) = e \chi v_0 \mathcal{G}_s \frac{\mathbf{B} - 2 \hat{\mathbf{k}} (\hat{\mathbf{k}} \cdot \mathbf{B})}{k^2}, \quad (9)$$

where  $\xi_s(\mathbf{k})$  and  $\mathbf{w}_s(\mathbf{k})$  are the OMM-modified energy and band velocity of the quasiparticles, respectively. With the usual usage of notations,  $\hat{\mathbf{k}}$  is the unit vector along  $\mathbf{k}$ . The full rotational isotropy of the Fermi surface, for each band of the RSW node, is broken by the inclusion of the OMM corrections.

### B. Chern numbers

Using Eq. (6), the Chern number for the  $s^{\text{th}}$  band can be evaluated as

$$\mathcal{C}_s = \frac{1}{2\pi} \int_S d\mathbf{S} \cdot \boldsymbol{\Omega}_s, \quad (10)$$

where  $S$  denotes a closed surface enclosing the  $\mathbf{k} = \mathbf{0}$  point and  $d\mathbf{S}$  denotes the outwardly-directed area vector for an infinitesimal patch on  $S$ . Exploiting the spherical symmetry of the Fermi surfaces for the bands of an isotropic RSW node, we can choose  $S$  to be the surface of a unit sphere. Expressing in terms of the spherical polar coordinates, we use  $k_x = \sin \theta \cos \phi$ ,  $k_y = \sin \theta \sin \phi$ , and  $k_z = \cos \theta$ , which gives us  $d\mathbf{S} = \sin \theta d\theta d\phi \hat{\mathbf{k}}$ . This leads to

$$\mathcal{C}_s = -\frac{\chi s}{2\pi} \int_S d\theta d\phi \sin \theta = -2 \chi s. \quad (11)$$

## III. QUANTIZATION OBSERVED IN NONLINEAR RESPONSE

In this section, we will unravel the quantized nature of the ECR and the TCR, associated with the electric and thermal currents, respectively, as explained in the introduction. The reader is referred to Appendix A for a detailed derivation of the forms of the electric and thermal current densities, denoted by  $\mathbf{J}_s$  and  $\mathbf{J}_s^{\text{th}}$ , respectively, starting from the Boltzmann equations. The final expressions are obtained by solving for  $\delta f_s(\mathbf{r}, \mathbf{k})$  [defined in Eq. (A15)], which is the deviation of the distribution of the quasiparticles from the equilibrium, upto second order in  $\epsilon$ . Here,  $\epsilon \in [0, 1]$  is perturbative parameter which quantifies the smallness of the magnitude of the probe fields comprising  $\mathbf{E}$ ,  $\nabla_{\mathbf{r}} T$ , and  $\nabla_{\mathbf{r}} \mu$ . In other words, we work in the regime where  $|\mathbf{E}| \propto \epsilon$ ,  $|\nabla_{\mathbf{r}} T| \propto \epsilon$ , and  $|\nabla_{\mathbf{r}} \mu| \propto \epsilon$ , and use the expression

$$f_s(\mathbf{r}, \mathbf{k}) = f_0(\varepsilon_s) + \epsilon f_s^{(1)}(\varepsilon_s) + \epsilon^2 f_s^{(2)}(\varepsilon_s) + \mathcal{O}(\epsilon^3) \quad (12)$$

in a perturbative expansion. Finally, we set  $\epsilon = 1$  at the end of our computations.

### A. Electrochemical response

For computing the ECR, we set  $\mathbf{B}$  and  $\nabla_{\mathbf{r}}T$  to zero. The part of the total electrical current density ( $\mathbf{J}_s$ ), which shows a quadratic dependence on the probe fields  $\mathbf{E}$  and  $\nabla_{\mathbf{r}}\mu$ , is denoted by  $\bar{\mathbf{J}}^s$ . This is the electrochemical current density, with its components being proportional to the quadratic combinations of the form  $E_a \partial_b \mu$ . Its  $a^{\text{th}}$  components is given by

$$\bar{J}_a^s = \vartheta_{abc}^s \partial_b \mu E_c, \quad (13)$$

where  $\vartheta_{abc}^s$  is a rank-three conductivity tensor for the  $s^{\text{th}}$  band (associated with the node of chirality  $\chi$ ). The dependence of the electric current on the the probe fields at second order is the reason why we call the response to be nonlinear.

For computing  $\vartheta_{abc}^s$ , we find that the solutions turn out to be

$$f_s^{(1)}(\varepsilon_s) = e \tau (\mathbf{v}_s \cdot \mathbf{E}) f_0'(\varepsilon_s), \quad f_s^{(2)}(\varepsilon_s) = e \tau [(\mathcal{E} \times \boldsymbol{\Omega}_s) \cdot \nabla_{\mathbf{r}}\mu] f_0'(\varepsilon_s) = e \tau [(\mathbf{E} \times \boldsymbol{\Omega}_s) \cdot \nabla_{\mathbf{r}}\mu] f_0'(\varepsilon_s), \quad (14)$$

where

$$\mathcal{E}(\mathbf{r}) = \mathbf{E} - \frac{\nabla_{\mathbf{r}}\mu(\mathbf{r})}{e}. \quad (15)$$

Due to the missing of the term  $\nabla_{\mathbf{r}}\mu$  in the BE by the authors in Ref. [61] [cf. Eq. (A5)], our solutions differ from theirs. Plugging in the solution in Eq. (A11), we obtain

$$\mathbf{J}_s = -e \int \frac{d^3\mathbf{k}}{(2\pi)^3} [\mathbf{v}_s f_0(\varepsilon_s) + e (\mathcal{E} \times \boldsymbol{\Omega}_s) f_0(\varepsilon_s)] - e^2 \tau \int \frac{d^3\mathbf{k}}{(2\pi)^3} [(e \mathbf{E} - \nabla_{\mathbf{r}}\mu) \times \boldsymbol{\Omega}_s (\mathbf{v}_s \cdot \mathbf{E}) + \mathbf{v}_s \{(\mathbf{E} \times \boldsymbol{\Omega}_s) \cdot \nabla_{\mathbf{r}}\mu\}] f_0'(\varepsilon_s). \quad (16)$$

The second term in the final expression is second-order in the probe fields, leading to

$$\bar{\mathbf{J}}^s = \mathbf{J}^{(s,1)} + \mathbf{J}^{(s,2)} + \mathbf{J}^{(s,3)}, \quad (17)$$

where

$$\begin{aligned} \mathbf{J}^{(s,1)} &= e^2 \tau \int \frac{d^3\mathbf{k}}{(2\pi)^3} (\nabla_{\mathbf{r}}\mu \times \boldsymbol{\Omega}_s) (\mathbf{v}_s \cdot \mathbf{E}) f_0'(\varepsilon_s), \quad \mathbf{J}^{(s,2)} = -e^2 \tau \int \frac{d^3\mathbf{k}}{(2\pi)^3} \mathbf{v}_s [(\mathbf{E} \times \boldsymbol{\Omega}_s) \cdot \nabla_{\mathbf{r}}\mu] f_0'(\varepsilon_s), \\ \mathbf{J}^{(s,3)} &= \frac{e^2 \tau \mathcal{G}_s}{s^2} \int \frac{d^3\mathbf{k}}{(2\pi)^3} \varepsilon_s (\mathbf{v}_s \cdot \mathbf{E}) (\boldsymbol{\Omega}_s \times \nabla_{\mathbf{r}}\mu) f_0''(\varepsilon_s). \end{aligned} \quad (18)$$

Here,  $\mathbf{J}^{(s,3)}$  represents the part arising from the magnetization density. We include it here, although it does not contribute to transport measurements, to outline its quantized nature (in the absence of tilt). On analyzing the form of  $\mathbf{J}^{(s,2)}$ , we find that a nonzero response is obtained when  $\mathbf{E}$  is oriented perpendicular to  $\nabla_{\mathbf{r}}\mu$ , and only the component of  $\boldsymbol{\Omega}_{s_2}$  which is perpendicular to both  $\mathbf{E}$  and  $\nabla_{\mathbf{r}}\mu$ , will contribute. Now, for an untilted RSW node, we find that  $\mathbf{v}_s \propto \boldsymbol{\Omega}_s \propto \hat{\mathbf{k}}$ . This immediately tells us that the integral will give a nonzero answer only from the component of  $\boldsymbol{\Omega}_s$  which is parallel to the current density, i.e.,  $J_a^{(s,2)} \propto \epsilon_{abc} \int d^3\mathbf{k} (v_s)_a (\Omega_s)_a \partial_b \mu E_c$ . An analogous argument for  $\mathbf{J}^{(s,1)}$  tells us that  $J_a^{(s,1)} \propto \epsilon_{abc} \int d^3\mathbf{k} (v_s)_a (\Omega_s)_a \partial_b \mu E_c$ .

The corresponding components of the third-rank conductivity tensors are given by

$$\begin{aligned} \vartheta_{abc}^{(s,1)} &= e^2 \tau \sum_d \epsilon_{abd} \int \frac{d^3\mathbf{k}}{(2\pi)^3} (v_s)_c (\Omega_s)_d f_0'(\varepsilon_s), \quad \vartheta_{abc}^{(s,2)} = -e^2 \tau \sum_d \epsilon_{bcd} \int \frac{d^3\mathbf{k}}{(2\pi)^3} (v_s)_a (\Omega_s)_d f_0'(\varepsilon_s), \\ \text{and } \vartheta_{abc}^{(s,3)} &= \frac{e^2 \tau \mathcal{G}_s}{s^2} \sum_d \epsilon_{adb} \int \frac{d^3\mathbf{k}}{(2\pi)^3} \varepsilon_s (v_s)_c (\Omega_s)_d f_0''(\varepsilon_s), \text{ such that } \bar{\vartheta}_{abc}^s = \vartheta_{abc}^{(s,1)} + \vartheta_{abc}^{(s,2)} + \vartheta_{abc}^{(s,3)}. \end{aligned} \quad (19)$$

For an untilted RSW node, we find that  $\mathbf{v}_s \propto \boldsymbol{\Omega}_s \propto \hat{\mathbf{k}}$ . This immediately tells us that the integral must be proportional to (1)  $\delta_{cd}$  for  $\vartheta_{abc}^{(s,1)}$  and  $\vartheta_{abc}^{(s,3)}$ ; (2)  $\delta_{ad}$  for  $\vartheta_{abc}^{(s,2)}$ . This gets rid of the summation over  $d$ , leading to

$$\vartheta_{abc}^{(s,1)} = e^2 \tau \epsilon_{abc} I_{s,c}^{(1)}, \quad \vartheta_{abc}^{(s,2)} = -e^2 \tau \epsilon_{abc} I_{s,a}^{(1)}, \quad \vartheta_{abc}^{(s,3)} = -\frac{e^2 \tau \mathcal{G}_s}{s^2} \epsilon_{abc} I_{s,c}^{(2)}, \quad (20)$$

where

$$I_{s,a}^{(1)} \equiv \int \frac{d^3\mathbf{k}}{(2\pi)^3} (v_s)_a (\Omega_s)_a f_0'(\varepsilon_s) \text{ and } I_{s,a}^{(2)} \equiv \int \frac{d^3\mathbf{k}}{(2\pi)^3} \varepsilon_s (v_s)_a (\Omega_s)_a f_0''(\varepsilon_s). \quad (21)$$

We employ the coordinate transformations shown in Eq. (B2). Using Eqs. (11), (B5), (B6), and (B7), we conclude that  $I_{s,x}^{(1)} = I_{s,y}^{(1)} = I_{s,z}^{(1)} = \mathcal{I}_s^{(1)}/3$  and  $I_{s,x}^{(2)} = I_{s,y}^{(2)} = I_{s,z}^{(2)} = \mathcal{I}_s^{(2)}/3$  where

$$\mathcal{I}_s^{(1)} = -\frac{\mathcal{C}_s}{(2\pi)^2} \text{ and } \mathcal{I}_s^{(2)} = -\mathcal{I}_s^{(1)}. \quad (22)$$

Plugging these in, we find the final expressions as follows:

$$\vartheta_{abc}^{(s,1)} = -\vartheta_{abc}^{(s,2)} = \frac{\epsilon_{abc} e^2 \tau}{3} \mathcal{I}_s^{(1)}, \quad \vartheta_{abc}^{(s,3)} = \frac{e^2 \tau \mathcal{G}_s}{3s^2} \epsilon_{abc} \mathcal{I}_s^{(1)}. \quad (23)$$

Therefore, each of the response coefficients is proportional to the Chern number, irrespective of the values of  $\mu$  and  $T$ , and, hence, show a completely quantized nature. Also, the nonzero response coefficients are the ones which are proportional to  $\epsilon_{abc}$ , representing the condition that  $\mathbf{J}^s \propto \mathbf{E} \times \nabla_{\mathbf{r}}\mu$  (i.e., the ones arising when the components of the electric current vector,  $\mathbf{E}$ , and  $\nabla_{\mathbf{r}}\mu$  are oriented orthogonal to each other). It is important to note that for nonzero tilt, although the leading-order terms (on expanding in  $|\eta| \ll 1$ ) take the quantized forms as shown above, nonzero subleading terms are generated, which are  $\eta$ -dependent. A nonzero  $\eta$  also generates nonzero components beyond those  $\propto \epsilon_{abc}$ .

## B. Thermochemical response

For computing the TCR, we set  $\mathbf{B}$  and  $\mathbf{E}$  to zero. The part of the total thermal current density ( $\mathbf{J}_s^{\text{th}}$ ), which shows a quadratic dependence on the probe fields  $\nabla_{\mathbf{r}}T$  and  $\nabla_{\mathbf{r}}\mu$ , is denoted by  $\mathbf{J}^{\text{th},s}$ . This is the thermochemical current density, with its components being proportional to the quadratic combinations of the form  $-\partial_a T \partial_b \mu$ . Its  $a^{\text{th}}$  components is given by

$$\bar{J}_a^{\text{th},s} = \varphi_{abc}^s \partial_b \mu (-\partial_c T), \quad (24)$$

where  $\varphi_{abc}^s$  is a rank-three thermal-conductivity tensor for the  $s^{\text{th}}$  band (associated with the node of chirality  $\chi$ ). The dependence of the thermal current on the the probe fields at second order is the reason why this response is nonlinear.

For computing  $\delta\phi_{abc}^s$ , we find that the solutions turn out to be

$$f_s^{(1)}(\varepsilon_s) = \frac{\tau(\varepsilon_s - \mu)}{T} (\mathbf{v}_s \cdot \nabla_{\mathbf{r}}T) f_0'(\varepsilon_s), \quad f_s^{(2)}(\varepsilon_s) = \frac{\tau(\varepsilon_s - \mu)}{T} [(\nabla_{\mathbf{r}}T \times \boldsymbol{\Omega}_s) \cdot \nabla_{\mathbf{r}}\mu] f_0'(\varepsilon_s). \quad (25)$$

Analogous to the ECR case, we get

$$\bar{\mathbf{J}}^{\text{th},s} = \mathbf{J}^{\text{th},(s,1)} + \mathbf{J}^{\text{th},(s,2)} + \mathbf{J}^{\text{th},(s,3)}, \quad (26)$$

where

$$\begin{aligned} \mathbf{J}^{\text{th},(s,1)} &= -\frac{\tau}{T} \int \frac{d^3\mathbf{k}}{(2\pi)^3} (\varepsilon_s - \mu)^2 (\nabla_{\mathbf{r}}\mu \times \boldsymbol{\Omega}_s) (\mathbf{v}_s \cdot \nabla_{\mathbf{r}}T) f_0'(\varepsilon_s), \\ \mathbf{J}^{\text{th},(s,2)} &= \frac{\tau}{T} \int \frac{d^3\mathbf{k}}{(2\pi)^3} (\varepsilon_s - \mu)^2 [\mathbf{v}_s (\nabla_{\mathbf{r}}T \times \boldsymbol{\Omega}_s) \cdot \nabla_{\mathbf{r}}\mu] f_0'(\varepsilon_s), \\ \mathbf{J}^{\text{th},(s,3)} &= -\frac{\tau \mathcal{G}_s}{s^2 T} \int \frac{d^3\mathbf{k}}{(2\pi)^3} (\varepsilon_s - \mu) \varepsilon_s (\mathbf{v}_s \cdot \nabla_{\mathbf{r}}T) (\boldsymbol{\Omega}_s \times \nabla_{\mathbf{r}}\mu) [(\varepsilon_s - \mu) f_0''(\varepsilon_s) + f_0'(\varepsilon_s)]. \end{aligned} \quad (27)$$

Here,  $\mathbf{J}^{\text{th},(s,3)}$  represents the part arising from the magnetization density.

The corresponding components of the third-rank thermal conductivity tensors are given by

$$\begin{aligned} \varphi_{abc}^{(s,1)} &= \frac{\tau}{T} \sum_d \int \frac{d^3\mathbf{k}}{(2\pi)^3} (\varepsilon_s - \mu)^2 \epsilon_{abd} (v_s)_c (\Omega_s)_d f_0'(\varepsilon_s), \\ \varphi_{abc}^{(s,2)} &= -\frac{\tau}{T} \sum_d \int \frac{d^3\mathbf{k}}{(2\pi)^3} (\varepsilon_s - \mu)^2 \epsilon_{bcd} (v_s)_a (\Omega_s)_d f_0'(\varepsilon_s), \text{ and} \\ \varphi_{abc}^{(s,3)} &= \frac{\tau \mathcal{G}_s}{T s^2} \sum_d \int \frac{d^3\mathbf{k}}{(2\pi)^3} (\varepsilon_s - \mu) \varepsilon_s \epsilon_{adb} (v_s)_c (\Omega_s)_d [(\varepsilon_s - \mu) f_0''(\varepsilon_s) + f_0'(\varepsilon_s)], \end{aligned}$$

$$\text{such that } \varphi_{abc}^s = \varphi_{abc}^{(s,1)} + \varphi_{abc}^{(s,2)} + \varphi_{abc}^{(s,3)}. \quad (28)$$



The relations  $\mathbf{v}_s \propto \boldsymbol{\Omega}_s \propto \hat{\mathbf{k}}$  for an untilted node again constrain the integrals to be proportional to (1)  $\delta_{cd}$  for  $\varphi_{abc}^{(s,1)}$  and  $\varphi_{abc}^{(s,3)}$ ; (2)  $\delta_{ad}$  for  $\varphi_{abc}^{(s,2)}$ . Hence, we get rid of the summation over  $d$ , leading to

$$\varphi_{abc}^{(s,1)} = \frac{\tau \epsilon_{abc}}{T} I_{s,c}^{(3)}, \quad \varphi_{abc}^{(s,2)} = -\frac{\tau \epsilon_{abc}}{T} I_{s,a}^{(3)}, \quad \varphi_{abc}^{(s,3)} = -\frac{\tau \mathcal{G}_s \epsilon_{abc}}{T s^2} I_{s,c}^{(4)}. \quad (29)$$

where

$$I_{s,a}^{(3)} \equiv \int \frac{d^3 \mathbf{k}}{(2\pi)^3} (\varepsilon_s - \mu)^2 (v_s)_a (\Omega_s)_a f'_0(\varepsilon_s) \text{ and } I_{s,a}^{(4)} \equiv \int \frac{d^3 \mathbf{k}}{(2\pi)^3} \varepsilon_s (v_s)_a (\Omega_s)_a \left[ (\varepsilon_s - \mu)^2 f''_0(\varepsilon_s) + (\varepsilon_s - \mu) f'_0(\varepsilon_s) \right]. \quad (30)$$

Employing Eqs. (B2), (11), (B5), (B6), and (B7), we conclude that  $I_{s,x}^{(3)} = I_{s,y}^{(3)} = I_{s,z}^{(3)} = \mathcal{I}_s^{(3)}/3$  and  $I_{s,x}^{(4)} = I_{s,y}^{(4)} = I_{s,z}^{(4)} = \mathcal{I}_s^{(4)}/3$  where

$$\mathcal{I}_s^{(3)} = -\frac{\pi^2 T^2 \mathcal{C}_s}{3 \times (2\pi)^2} = \frac{\pi^2 T^2}{3} \mathcal{I}_s^{(1)} \text{ and } \mathcal{I}_s^{(4)} = -\frac{2\pi^2 T^2}{3} \mathcal{I}_s^{(1)}. \quad (31)$$

Plugging these in, we find the final expressions as follows:

$$\varphi_{abc}^{(s,1)} = -\varphi_{abc}^{(s,2)} = \epsilon_{abc} \frac{\pi^2 T}{3} \tau \mathcal{I}_s^{(1)}, \quad \varphi_{abc}^{(s,3)} = \frac{2\pi^2 T}{3} \frac{\tau \mathcal{G}_s}{s^2} \epsilon_{abc} \mathcal{I}_s^{(1)}. \quad (32)$$

Clearly, the results are quantized only at a fixed value of  $T$ , as the overall response increases linearly with increasing  $T$ . Needless to say here that the nonzero response coefficients are the ones which are proportional to  $\epsilon_{abc}$ , representing the condition that  $\bar{\mathbf{J}}^{\text{th},s} \propto \nabla_{\mathbf{r}} T \times \nabla_{\mathbf{r}} \mu$  (i.e., the ones arising when the components of the thermal current vector,  $\nabla_{\mathbf{r}} T$ , and  $\nabla_{\mathbf{r}} \mu$  are oriented orthogonal to each other). Similar to the ECR case, for a nonzero tilt, in addition to the leading-order terms (on expanding in  $|\eta| \ll 1$ ) taking the quantized forms as shown above,  $\eta$ -dependent terms are generated. A nonzero  $\eta$  will also be responsible for giving rise to nonzero components beyond those  $\propto \epsilon_{abc}$ .

From Eqs. (23) and (32), we find that

$$\vartheta_{abc}^{(s,i)} = \frac{3 e^2}{\pi^2 T} \varphi_{abc}^{(s,i)} \quad (33)$$

is satisfied for  $i = 1$  and  $i = 3$ , which embodies the Wiedemann-Franz law [68]. However,  $\vartheta_{abc}^{(s,3)} = \frac{3 e^2}{2\pi^2 T} \varphi_{abc}^{(s,3)}$ . This is fine because the Wiedemann-Franz law is primarily applicable for linear response, and it is not universally valid in the nonlinear regimes (see, for example [69]).

#### IV. MAGNETOELECTRIC CONDUCTIVITY

In a planar Hall set-up comprising static uniform electric and magnetic fields applied parallel to each other, a nonzero tilt induces the linear response from an RSW node to contain parts which vary linearly with  $B$  (which we demonstrate below). In this section, our aim is to elucidate how the characteristic topological quantities arise in those linear-in- $B$  parts of the magnetoconductivity tensor.

In a planar Hall set-up, the magnetoelectric conductivity tensor is obtained from Eq. (A11), with the solution (see Ref. [36] for detailed derivations starting from the Boltzmann equations)

$$f_s(\mathbf{k}) = f_0(\xi_s) + \delta f_s(\mathbf{k}), \quad \delta f_s(\mathbf{k}) = [-f'_0(\xi_s)] g_s(\mathbf{k}), \quad \frac{g_s(\mathbf{k})}{e\tau} = -\sum_{n=0}^{\infty} (e\tau \mathcal{D}_s)^n \hat{L}^n [\mathcal{D}_s^{\chi} (\mathbf{w}_s^{\chi} + \mathbf{W}_s^{\chi}) \cdot \mathbf{E}], \quad (34)$$

where

$$\hat{L} = (\mathbf{w}_s^{\chi} \times \mathbf{B}) \cdot \nabla_{\mathbf{k}} \quad (35)$$

is referred to as the Lorentz operator (because it includes the classical effect due to the Lorentz force). We would like to point out here that, in Ref. [36], two of us have studied the question of linear response for planar Hall and planar thermal set-ups consisting of untilted RSW nodes (i.e.,  $\eta = 0$ ). As such, the response coefficients did not have any part having a linear-in- $B$  dependence. The fact that the linear-in- $B$  parts go to zero for  $\eta = 0$  [36] is expected because, according to the Onsager-Casimir reciprocity relations [33, 70–72], terms containing odd powers of  $B$  cannot arise in this situation. However, in the presence of a nonzero tilt, the conditions are relaxed, making it possible for the existence of terms varying linearly with  $B$  [33].

Here, we will consider that case when  $\mathbf{E}$  and  $\mathbf{B}$  are parallel to each other (see Ref. [73] for the same set-up applied to WSMs). Therefore, if  $\mathbf{E}$  is applied along the unit vector  $\hat{\mathbf{e}}_E$ , such that  $\mathbf{E} = E \hat{\mathbf{e}}_E$ , we have  $\mathbf{B} = B \hat{\mathbf{e}}_E$  and  $\zeta_s = -(m_s)_b B =$

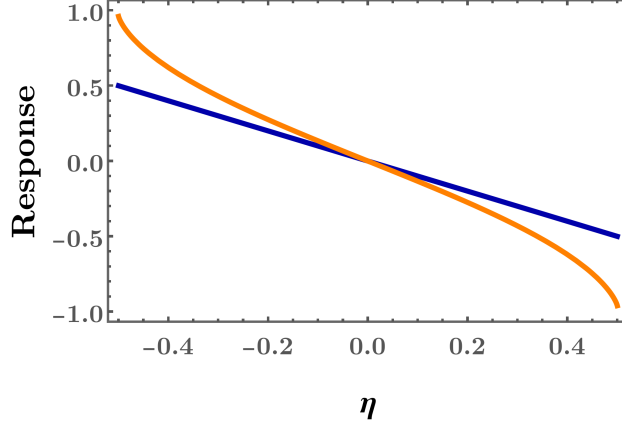


FIG. 2. Plots for  $\sum_{s=1/2,3/2} \frac{\eta \mathcal{C}_s}{4}$  (blue) and  $\sum_{s=1/2,3/2} \frac{\chi \mathcal{G}_s}{2} \frac{\eta s - (s^2 - \eta^2) \tanh^{-1}(\frac{\eta}{s})}{\eta^2}$  (orange) as functions of  $\eta$ , after setting  $\chi = +1$ . The behaviour for  $\chi = -1$  is obtained simply as the negative of the above curves.

$e \chi v_0 \mathcal{G}_s \frac{k_b B}{k^2}$  [cf. Eq. (8)]. We are primarily interested in finding the form of the part of the magnetoelectric conductivity tensor, denoted by  $(\sigma_s^{\text{lin}})_{ab}$ , which is linear-in- $B$ . Expressing the corresponding part of the current as  $J_a^{\text{lin},s} = (\sigma_s^{\text{lin}})_{ab} E^b$ , let us define a third-rank tensor

$$(\zeta_s^{\text{lin}})^c{}_{ab} = \frac{\partial (\sigma_s^{\text{lin}})_{ab}}{\partial B_c}. \quad (36)$$

For our scenario with  $\mathbf{E} \parallel \mathbf{B}$ , we will be dealing with the vector defined as

$$\zeta_a^s = \sum_{b,c} (\zeta_s^{\text{lin}})^c{}_{ab} \delta^b{}_c = \sum_b (\zeta_s^{\text{lin}})^b{}_{ab} \equiv \zeta_a^{(s,1)} + \zeta_a^{(s,2)} + \zeta_a^{(s,3)} + \zeta_a^{(s,4)} + \zeta_a^{(s,5)}, \quad (37)$$

where (see Appendix C for the intermediate steps)

$$\begin{aligned} \zeta_a^{(s,1)} &= e^3 \tau \int \frac{d^3 \mathbf{k}}{(2\pi)^3} (v_s)_a (\mathbf{v}_s \cdot \boldsymbol{\Omega}_s) f'_0(\varepsilon_s) = -\frac{\delta_{za} \eta v_0 e^3 \tau \mathcal{C}_s}{4\pi^2}, \quad \zeta_a^{(s,2)} = -4\zeta_a^{(s,1)}, \\ \zeta_a^{(s,3)} &= \frac{e^3 \tau v_0 \mathcal{G}_s}{s} \int \frac{d^3 \mathbf{k}}{(2\pi)^3} (v_s)_a [\nabla_{\mathbf{k}} \cdot (k \boldsymbol{\Omega}_s)] f'_0(\varepsilon_s) = -\frac{\delta_{za} \chi v_0 e^3 \tau \mathcal{G}_s}{2\pi^2} \frac{(s^2 - \eta^2) \tanh^{-1}(\frac{\eta}{s}) - \eta s}{\eta^2} \text{ for } |\eta| < |s|, \\ \zeta_a^{(s,4)} &= \frac{e^3 \tau v_0 \mathcal{G}_s}{s} \int \frac{d^3 \mathbf{k}}{(2\pi)^3} [\mathbf{v}_s \cdot \partial_{k_a} (k \boldsymbol{\Omega}_s)] f'_0(\varepsilon_s) = \zeta_a^{(s,3)}, \quad \zeta_a^{(s,5)} = \frac{e^3 \tau v_0 \mathcal{G}_s}{s} \int \frac{d^3 \mathbf{k}}{(2\pi)^3} (v_s)_a k (\mathbf{v}_s \cdot \boldsymbol{\Omega}_s) f''_0(\varepsilon_s) = -\zeta_a^{(s,3)}. \end{aligned} \quad (38)$$

Appendix C4 provides more details regarding the steps leading to the final expressions shown above. Here,  $\zeta_a^{(s,1)}$  and  $\zeta_a^{(s,2)}$  represent the parts arising purely from the BC (i.e., with no contribution from the OMM),  $\zeta_a^{(s,3)}$ ,  $\zeta_a^{(s,4)}$ , and  $\zeta_a^{(s,5)}$  are the terms which go to zero if OMM is neglected. Some comments are in order:

1. We find that all the above response coefficients go to zero for  $\eta = 0$ , validating our arguments that the linear-in- $B$  terms do not survive in the limit of zero tilt.
2. Since  $\zeta_a^{(s,1)}$  and  $\zeta_a^{(s,2)}$  are proportional to  $\eta \mathcal{C}_s$ , not depending on  $\mu$  and  $T$ , they reflect a robust quantized response. Hence, it is easy to identify this part of the response irrespective of the specific material one chooses to study in experiments. The corresponding linear-in- $\eta$  behaviour is illustrated in Fig. 2 (blue line).
3. Although  $\zeta_a^{(s,3)}$ ,  $\zeta_a^{(s,4)}$ , and  $\zeta_a^{(s,5)}$  are proportional to  $\chi \mathcal{G}_s$ , and are independent of  $\mu$  and  $T$ , they have a complicated (nonlinear) dependence on  $\eta$ . Since  $\eta$  a nonuniversal parameter, changing its value according to the material under consideration, it is then hard to disentangle/extract the feature of  $\mathcal{G}_s$ -proportionality. The corresponding nonlinear behaviour is illustrated in Fig. 2 (orange curve).

## V. SUMMARY AND FUTURE PERSPECTIVES

In this paper, we have considered the response coefficients in two distinct experimental set-ups, with the intent of identifying clear signatures of the topological features of the bandstructures of nodal-point semimetals, by taking RSW



semimetal as an example. In the first case, the response is nonlinear in nature, arising under the combined effects of an external electric field (and/or temperature gradient) and the gradient of the chemical potential. When internode scatterings can be ignored, the relaxation-time approximation leads to the ECR and TCR taking a quantized value for a single untilted RSW node, insensitive to the specific values of the chemical potential and the temperature. The second case investigates the linear-response coefficient in the form of the magnetoelectric conductivity under the action of collinear electric and magnetic fields, resulting in a planar Hall set-up. In particular, we have considered the nature of the linear-in- $B$  parts of the conductivity tensor, which are nonvanishing only in the presence of a nonzero tilt. We find that the components show a quantized nature with coefficients which are functions of  $\eta$ .

The advantage of considering RSW semimetals is that it provides a richer structure for demonstrating the topological features contained in the response coefficients, compared to the WSMs, because of the fact that the former consists of four bands (rather than just two). Basically, each band has its distinct topological features, reflected by the band-dependent values of the BC and the OMM. Through our band-dependent results for the relevant response coefficients, we have, thus, succeeded in chalking out the signatures of these individual bands. In the future, it will be worthwhile to calculate the behaviour of the response coefficients in situations where internode scatterings cannot be ignored [36]. Furthermore, it will be interesting to investigate the effects of anisotropy/disorder [5, 6, 74] and/or strong interactions on the quantized nature of the response [10].

### DATA AVAILABILITY STATEMENT

Data sharing is not applicable to this article as no new data were created or analyzed in this study.

### Appendix A: Response resulting from the Boltzmann equations

In this appendix, we will outline the semiclassical Boltzmann equation (BE) formalism [32, 34, 36], which is used here for determining the transport coefficients. This framework is applicable in the regime of small deviations from the equilibrium quasiparticle distribution. If there is an externally-applied magnetic field  $\mathbf{B}$ , then we will assume that it is of small in magnitude, associated with a small cyclotron frequency  $\omega_c = eB/(m^*c)$  (where  $m^*$  is the effective mass with the magnitude  $\sim 0.11m_e$  [75], with  $m_e$  denoting the electron mass). This condition is necessary when we want to focus on the regime where quantized Landau levels need not be considered, given by the inequality  $\hbar\omega_c \ll \mu$ , where  $\mu$  is the chemical potential cutting the energy band(s), thus defining the Fermi-energy level. Here, we will approximate the form of the collision integral with a relaxation time ( $\tau$ ), which is a momentum-independent phenomenological parameter. Furthermore, we will focus on the limit when only intranode scatterings dominate in the collision processes, such that  $\tau$  corresponds exclusively to the intranode scattering time. Hence, it is sufficient to derive the relevant expressions for a single node, whose chirality is denoted by  $\chi$ .

For a 3d system, we define the Fermi-Dirac distribution function  $f_s(\mathbf{r}, \mathbf{k}, t)$  for the quasiparticles occupying a Bloch band labelled by the index  $s$ , with the crystal momentum  $\mathbf{k}$  and dispersion  $\varepsilon_s(\mathbf{k})$ , such that  $dN_s = g_s f_s(\mathbf{r}, \mathbf{k}, t) \frac{d^3\mathbf{k}}{(2\pi)^3} d^3\mathbf{r}$  is the number of particles occupying an infinitesimal phase space volume of  $dV_p = \frac{d^3\mathbf{k}}{(2\pi)^3} d^3\mathbf{r}$ , centered at  $\{\mathbf{r}, \mathbf{k}\}$  at time  $t$ . Here,  $g_s$  denotes the degeneracy of the band. We define the OMM-corrected dispersion and the corresponding modified Bloch velocity as

$$\xi_s(\mathbf{k}) = \varepsilon_s(\mathbf{k}) + \zeta_s(\mathbf{k}) \text{ and } \mathbf{w}_s(\mathbf{k}) = \nabla_{\mathbf{k}}\varepsilon_s(\mathbf{k}) + \nabla_{\mathbf{k}}\zeta_s(\mathbf{k}), \quad (\text{A1})$$

respectively.

It is convenient to introduce a combined electrochemical potential  $\Phi(\mathbf{r}) + \frac{\mu(\mathbf{r})}{e}$ , giving rise to a generalized (external) force field defined by

$$\mathcal{E}(\mathbf{r}) = -\nabla_{\mathbf{r}} \left[ \Phi(\mathbf{r}) + \frac{\mu(\mathbf{r})}{e} \right], \quad \mathbf{E} = -\nabla_{\mathbf{r}}\Phi, \quad (\text{A2})$$

where  $\Phi(\mathbf{r})$  is the scalar potential. The Hamilton's equations of motion for the quasiparticles, under the influence of a static electrochemical potential and a static magnetic ( $\mathbf{B}$ ) field, are given by [68, 76, 77]

$$\begin{aligned} \dot{\mathbf{r}} &= \nabla_{\mathbf{k}}\xi_s - \dot{\mathbf{k}} \times \boldsymbol{\Omega}_s \text{ and } \dot{\mathbf{k}} = -e(\mathcal{E} + \dot{\mathbf{r}} \times \mathbf{B}) \\ \Rightarrow \dot{\mathbf{r}} &= \mathcal{D}_s [\mathbf{w}_s + e(\mathcal{E} \times \boldsymbol{\Omega}_s) + e(\boldsymbol{\Omega}_s \cdot \mathbf{w}_s)\mathbf{B}] \text{ and } \dot{\mathbf{k}} = -e\mathcal{D}_s [\mathcal{E} + (\mathbf{w}_s \times \mathbf{B}) + e(\mathcal{E} \cdot \mathbf{B})\boldsymbol{\Omega}_s]. \end{aligned} \quad (\text{A3})$$

where  $-e$  is the charge carried by each quasiparticle. Furthermore,

$$\mathcal{D}_s = \frac{1}{1 + e(\mathbf{B} \cdot \boldsymbol{\Omega}_s)} \quad (\text{A4})$$

is the factor which modifies the phase volume element from  $dV_p$  to  $(\mathcal{D}_s)^{-1} dV_p$ , such that the Liouville's theorem (in the absence of collisions) continues to hold in the presence of a nonzero BC [78–81]. Putting everything together, the BE for the quasiparticles takes the form [21, 82]

$$\mathcal{D}_s \left[ \partial_t + \{ \mathbf{w}_s + e \boldsymbol{\mathcal{E}} \times \boldsymbol{\Omega}_s + e (\boldsymbol{\Omega}_s \cdot \mathbf{w}_s) \mathbf{B} \} \cdot \nabla_{\mathbf{r}} - e (\boldsymbol{\mathcal{E}} + \mathbf{w}_s \times \mathbf{B}) \cdot \nabla_{\mathbf{k}} - e^2 (\boldsymbol{\mathcal{E}} \cdot \mathbf{B}) \boldsymbol{\Omega}_s \cdot \nabla_{\mathbf{k}} \right] f_s = I_{\text{coll}}. \quad (\text{A5})$$

which results from the Liouville's equation in the presence of scattering events. On the right-hand side,  $I_{\text{coll}}$  denotes the collision integral, which corrects the Liouville's equation, taking into account the collisions of the quasiparticles. We would like to point out that the term represented by  $\nabla_{\mathbf{r}} \mu$  was missed in Ref. [61], which demonstrated the quantized ECR in Weyl semimetals.

Let the contributions to the average DC electric and thermal current densities from the quasiparticles, associated with the band  $s$  at the node with chirality  $\chi$ , be  $\mathbf{J}_s$  and  $\mathbf{J}_s^{\text{th}}$ , respectively. The linear-response matrix, which relates the resulting generalized current densities to the driving electric potential gradient and temperature gradient, is expressed as

$$\begin{bmatrix} (J_s)_a \\ (J_s^{\text{th}})_a \end{bmatrix} = \sum_b \begin{bmatrix} (\sigma_s)_{ab} & (\alpha_s)_{ab} \\ T(\alpha_s)_{ab} & (\ell_s)_{ab} \end{bmatrix} \begin{bmatrix} E_b \\ -\partial_b T \end{bmatrix}, \quad (\text{A6})$$

where  $\{a, b\} \in \{x, y, z\}$  indicates the Cartesian components of the current density vectors and the response tensors in 3d. The symbols  $\sigma_s$  and  $\alpha_s$  represents the magnetoelectric conductivity and the magnetothermoelectric conductivity tensors, respectively. The latter determines the Peltier ( $\Pi_s$ ), Seebeck ( $S_s$ ), and Nernst coefficients. The third tensor  $\ell$  represents the linear response relating the thermal current density to the temperature gradient, at a vanishing electric field.  $S$ ,  $\Pi$ , and the magnetothermal coefficient tensor  $\kappa$  (which provides the coefficients between the heat current density and the temperature gradient at vanishing electric current) are related as [34, 68]:

$$(S_s)_{ab} = \sum_{i'} (\sigma_s)_{aa'}^{-1} (\alpha_s)_{a'b}, \quad (\Pi_s)_{ab} = T \sum_{a'} (\alpha_s)_{aa'} (\sigma_s)_{a'b}^{-1}, \quad (\kappa_s)_{ab} = (\ell_s)_{ab} - T \sum_{a', b'} (\alpha_s)_{aa'} (\sigma_s)_{a'b'}^{-1} (\alpha_s)_{b'b}. \quad (\text{A7})$$

Since  $\ell_s$  determines the first term in the magnetothermal coefficient tensor  $\kappa_s$ , here we will loosely refer to  $\ell_s$  itself as the magnetothermal coefficient.

The explicit form of the dc charge current density is given by [67, 83, 84]

$$\mathbf{J}_s^{\text{tot}} = -e g_s \int \frac{d^3 \mathbf{k}}{(2\pi)^3} \mathcal{D}_s^{-1} \dot{\mathbf{r}} f_s(\mathbf{r}, \mathbf{k}) + \nabla_{\mathbf{r}} \times \mathbf{M}_s(\mathbf{r}), \quad \mathbf{M}_s(\mathbf{r}) = g_s \int \frac{d^3 \mathbf{k}}{(2\pi)^3} \mathcal{D}_s^{-1} \mathbf{m}_s(\mathbf{k}) f_s(\mathbf{r}, \mathbf{k}), \quad (\text{A8})$$

where  $\mathbf{M}_s(\mathbf{r})$  is the magnetization density. As discussed earlier,  $\mathbf{m}_s(\mathbf{k})$  represents the the orbital magnetic moment, which generically describes the rotation of a wavepacket around its center of mass. The contribution from the magnetic moments to the local current density must be subtracted out in the transport current, because the magnetization current cannot be measured by conventional transport experiments [85]. Therefore, the transport current is defined by  $\mathbf{J}_s = \mathbf{J}_s^{\text{tot}} - g_s \nabla_{\mathbf{r}} \times \int \frac{d^3 \mathbf{k}}{(2\pi)^3} \mathcal{D}_s^{-1} \mathbf{m}_s(\mathbf{k}) f_s(\mathbf{r}, \mathbf{k})$ , leading to

$$\mathbf{J}_s = -e g_s \int \frac{d^3 \mathbf{k}}{(2\pi)^3} \mathcal{D}_s^{-1} \dot{\mathbf{r}} f_s(\mathbf{r}, \mathbf{k}). \quad (\text{A9})$$

In an analogous way, the transport heat current is captured by [83]

$$\mathbf{J}_s^{\text{th}} = g_s \int \frac{d^3 \mathbf{k}}{(2\pi)^3} (\mathcal{D}_s)^{-1} \dot{\mathbf{r}} (\xi_s - \mu) f_s^\chi(\mathbf{r}, \mathbf{k}). \quad (\text{A10})$$

Plugging in the expressions shown in in Eq. (A3), we get

$$\begin{aligned} \mathbf{J}_s &= -e g_s \int \frac{d^3 \mathbf{k}}{(2\pi)^3} [\mathbf{w}_s + e (\boldsymbol{\mathcal{E}} \times \boldsymbol{\Omega}_s) + e (\boldsymbol{\Omega}_s \cdot \mathbf{w}_s) \mathbf{B}] f_s(\mathbf{r}, \mathbf{k}) \\ \text{and } \mathbf{J}_s^{\text{th}} &= g_s \int \frac{d^3 \mathbf{k}}{(2\pi)^3} [\mathbf{w}_s + e (\boldsymbol{\mathcal{E}} \times \boldsymbol{\Omega}_s) + e (\boldsymbol{\Omega}_s \cdot \mathbf{w}_s) \mathbf{B}] (\xi_s - \mu) f_s(\mathbf{r}, \mathbf{k}). \end{aligned} \quad (\text{A11})$$

Under the relaxation-time approximation, the collision integral takes the form of

$$I_{\text{coll}} = \frac{f_s^{(0)}(\mathbf{r}, \mathbf{k}) - f_s(\mathbf{r}, \mathbf{k}, t)}{\tau}, \quad (\text{A12})$$

where the time-independent distribution function

$$f_s^{(0)}(\mathbf{r}, \mathbf{k}) \equiv f_0(\xi_s(\mathbf{k}), \mu, T(\mathbf{r})) = \frac{1}{1 + \exp\left[\frac{\xi_s(\mathbf{k}) - \mu}{T(\mathbf{r})}\right]}, \quad (\text{A13})$$

describes a local equilibrium situation at the subsystem centred at position  $\mathbf{r}$ , at the local temperature  $T(\mathbf{r})$ , and with a local chemical potential  $\mu$ . The gradients of the equilibrium distribution function evaluate to

$$\nabla_{\mathbf{k}} f_0(\xi_s) = \mathbf{w}_s f_0'(\xi_s) \text{ and } \nabla_{\mathbf{r}} f_0(\xi_s) = - \left[ \nabla_{\mathbf{r}} \mu + (\xi_s - \mu) \frac{\nabla_{\mathbf{r}} T}{T} \right] f_0'(\xi_s), \quad (\text{A14})$$

where the ‘‘prime’’ superscript is used to indicate partial-differentiation with respect to the variable shown within the brackets [for example,  $f_0'(u) \equiv \partial_u f_0(u)$ ]. Henceforth, we set  $g_s = 1$ , ignoring the degeneracy due to electron’s spin.

In order to obtain a solution to the full BE, for small time-independent values of  $\mathbf{E}$ ,  $\nabla_{\mathbf{r}} T$ , and  $\nabla_{\mathbf{r}} \mu$ , we assume a small deviation from the equilibrium distribution of the quasiparticles, such that

$$f_s(\mathbf{r}, \mathbf{k}, t) \equiv f_s(\mathbf{r}, \mathbf{k}) = f_0 + \delta f_s(\mathbf{r}, \mathbf{k}). \quad (\text{A15})$$

Here, we have not included any explicit time-dependence in  $\delta f_s(\mathbf{r}, \mathbf{k})$  because the applied fields and gradients are static. Furthermore, we have suppressed showing explicitly the dependence of  $f_0$  on  $\xi_s(\mathbf{k})$ ,  $\mu$ , and  $T(\mathbf{r})$ . We now parametrize the deviation as  $\delta f_s(\mathbf{r}, \mathbf{k}) = \sum_{p=1}^{\infty} \epsilon^p f_s^{(p)}$ , where  $\epsilon \in [0, 1]$  is the perturbative parameter having the same order of smallness as the external perturbations  $\mathbf{E}$ ,  $\nabla_{\mathbf{r}} T$ , and  $\nabla_{\mathbf{r}} \mu$ . Since  $\epsilon$  is used solely for bookkeeping purpose (to track the order in the degree of smallness), we will set  $\epsilon = 1$  at the end of the calculations after we solve for  $\delta f_s(\mathbf{r}, \mathbf{k})$  recursively, order by order in increasing powers of  $\epsilon$ .

## Appendix B: Useful integrals

In the main text, we have to deal with integrals of the form:

$$\mathcal{I} = \int \frac{d^3 \mathbf{k}}{(2\pi)^3} F(\mathbf{k}, \varepsilon_s) f_0'(\varepsilon_s), \quad (\text{B1})$$

where  $\varepsilon_s = s v_0 k + v_0 \eta k_z$ . We switch to the spherical polar coordinates such that

$$k_x = \frac{\tilde{\varepsilon} \cos \phi \sin \theta}{s v_0}, \quad k_y = \frac{\tilde{\varepsilon} \sin \phi \sin \theta}{s v_0}, \quad k_z = \frac{\tilde{\varepsilon} \cos \theta}{s v_0}, \quad (\text{B2})$$

where  $\tilde{\varepsilon} \in [0, \infty)$ ,  $\phi \in [0, 2\pi)$ , and  $\theta \in [0, \pi]$ . The Jacobian of the transformation is  $\mathcal{J}(\tilde{\varepsilon}, \theta) = \frac{\tilde{\varepsilon}^2 \sin \theta}{s^3 v_0^3}$ . This leads to

$$\int_{-\infty}^{\infty} d^3 \mathbf{k} \rightarrow \int_0^{\infty} d\tilde{\varepsilon} \int_0^{2\pi} d\phi \int_0^{\pi} d\theta \mathcal{J}(\tilde{\varepsilon}, \theta) \text{ and } \varepsilon_s(\mathbf{k}) \rightarrow \varepsilon_s(\tilde{\varepsilon}, \theta) = \tilde{\varepsilon} \Lambda_s(\theta), \text{ with } \Lambda_s(\theta) = 1 + \frac{\eta \cos \theta}{s}. \quad (\text{B3})$$

Since we have chosen the tilting direction with respect to the  $z$ -axis, the dispersion does not depend on  $\phi$ . Hence, we can perform the  $\phi$ -integration easily, after which  $\mathcal{I}$  can be written in the following schematic form:

$$\mathcal{I} = \int_0^{\infty} d\varepsilon \int_0^{\pi} d\theta \mathcal{I}_1(\varepsilon, \theta) f_0'(\varepsilon_s). \quad (\text{B4})$$

where  $\mathcal{I}_1(\varepsilon, \theta)$  is the function obtained after the  $\phi$ -integration.

In our computations, the  $\tilde{\varepsilon}$ - and  $\theta$ -dependent parts of the integrand are decoupled. Hence, let us discuss some generic identities for these two kinds of integrals. For the  $\tilde{\varepsilon}$ -integration, we encounter integrals of the forms  $\int_0^{\infty} d\tilde{\varepsilon} \tilde{\varepsilon}^n f_0'(\varepsilon_s)$  and  $\int_0^{\infty} d\tilde{\varepsilon} \tilde{\varepsilon}^n \frac{\partial^{\lambda+1} f_0(\varepsilon_s)}{\partial \varepsilon_s^{\lambda+1}}$ , where  $\{n, \lambda\} \in \{0, \mathbb{Z}^+\}$ . Applying the Sommerfeld expansion [68], we get

$$\int_0^{\infty} d\tilde{\varepsilon} \tilde{\varepsilon}^n f_0'(\varepsilon_s) = - \int_0^{\infty} d\tilde{\varepsilon} \tilde{\varepsilon}^n \frac{\beta e^{\beta(\varepsilon_s - \mu)}}{[1 + e^{\beta(\varepsilon_s - \mu)}]^2} = - \frac{1}{\Lambda_s^{n+1}(\theta)} \int_0^{\infty} d\tilde{\varepsilon} \tilde{\varepsilon}^n \frac{\beta e^{\beta(\tilde{\varepsilon} - \mu)}}{(1 + e^{\beta(\tilde{\varepsilon} - \mu)})^2} = - \frac{\Upsilon_n(\mu, T)}{\Lambda_s^{n+1}(\theta)}, \quad (\text{B5})$$

where

$$\Upsilon_n(\mu, T) = \mu^n \left[ 1 + \frac{\pi^2 T^2 n(n-1)}{6 \mu^2} + \frac{7 \pi^2 T^4 n(n-3)(n-2)(n-1)}{360 \mu^4} + \mathcal{O}\left(\left(\frac{\mu}{T}\right)^{-6}\right) \right], \quad (\text{B6})$$

which is valid in the regime  $\beta \mu \gg 1$  (or  $\mu \gg T$  in the natural units). It is easy to show that [35, 36], for higher-order derivatives, we have the relation

$$\int_0^{\infty} d\tilde{\varepsilon} \tilde{\varepsilon}^n (-1)^{\lambda+1} \frac{\partial^{\lambda+1} f_0(\tilde{\varepsilon})}{\partial \tilde{\varepsilon}^{\lambda+1}} = \frac{n!}{(n-\lambda)!} \frac{\Upsilon_{n-\lambda}(\mu, T)}{\Lambda_s^{n+1}(\theta)}. \quad (\text{B7})$$

For the  $\theta$ -integration, we use the identity

$$\begin{aligned} \int_0^\pi d\theta \frac{(\sin \theta)^m (\cos \theta)^n}{(s + \eta \cos \theta)^l} &= \int_{-1}^1 dt \frac{(1-t^2)^{\frac{m-1}{2}} t^n}{(s + \eta t)^l} \\ &= \frac{\sqrt{\pi} \Gamma(\frac{m+1}{2})}{4 s^l} \left[ 2 \{(-1)^n + 1\} \Gamma\left(\frac{n+1}{2}\right) {}_3\tilde{F}_2\left(\frac{n+1}{2}, \frac{l+1}{2}, \frac{l}{2}; \frac{1}{2}, \frac{1}{2}; \frac{\eta^2}{s^2}\right) \right. \\ &\quad \left. + \frac{\eta^l}{s} \{(-1)^n - 1\} \Gamma\left(\frac{n}{2} + 1\right) {}_3\tilde{F}_2\left(\frac{n+2}{2}, \frac{l+1}{2}, \frac{l+2}{2}; \frac{3}{2}, \frac{m+n+3}{2}; \frac{\eta^2}{s^2}\right) \right], \end{aligned} \quad (\text{B8})$$

where  ${}_n\tilde{F}_{n_2}(\{a_1, \dots, a_{n_1}\}; \{b_1, \dots, b_{n_2}\}; X)$  is the regularized hypergeometric function [86].

### Appendix C: Linear-in- $B$ parts of magnetoelectric conductivity

In this appendix, we outline the forms of the various components of the magnetoelectric conductivity tensor, involving the linear-in- $B$  parts, for the planar Hall set-up with  $\mathbf{E}$  and  $\mathbf{B}$  aligned parallel to each other (discussed in Sec. IV).

#### 1. Intrinsic anomalous-Hall part

From the term proportional to  $(\mathbf{E} \times \boldsymbol{\Omega}_s)$  in the integrand of Eq. (A11), we get the linear-response current density as

$$\mathbf{J}_s^{\text{AH}} = -e^2 \int \frac{d^3\mathbf{k}}{(2\pi)^3} [(\mathbf{E} \times \boldsymbol{\Omega}_s)] f_0(\xi_s), \quad (\text{C1})$$

which gives the intrinsic anomalous Hall term. Using  $f_0(\xi_s) = f_0(\varepsilon_s) + \zeta_s f'_0(\varepsilon_s) + \mathcal{O}(B^2)$ , we get

$$(\sigma_s^{\text{AH}})_{ab} = -e^2 \epsilon_{abc} \int \frac{d^3\mathbf{k}}{(2\pi)^3} (\Omega_s)^c [f_0(\varepsilon_s) + \zeta_s f'_0(\varepsilon_s) + \mathcal{O}(B^2)], \quad (\text{C2})$$

whose diagonal components are automatically zero because of the Levi-Civita symbol. A nonzero OMM may generate  $B$ -dependent terms in  $(\sigma_s^{\text{AH}})_{ab}$ .

For  $\eta = 0$ , the contribution from the first term vanishes identically. For  $\eta \neq 0$ , although we get nonzero components from this first term, they are  $B$ -independent and does not contribute to  $\zeta_a^s$ . Let us consider the second term in the integrand, which is proportional to  $\zeta_s f'_0(\varepsilon_s)$ . First let us assume that  $\hat{\mathbf{e}}_E = \hat{\mathbf{x}}$ , which involves setting  $\zeta_s = e \chi v_0 \mathcal{G}_s k_x B/k^2$ . The corresponding contribution to

1.  $(\sigma_s^{\text{AH}})_{yx}$  is

$$t_{yx} \equiv -e^3 \chi v_0 \mathcal{G}_s B \epsilon_{yxz} \int \frac{d^3\mathbf{k}}{(2\pi)^3} (\Omega_s)^z \frac{k_x}{k^2} f'_0(\varepsilon_s) = 0; \quad (\text{C3})$$

2.  $(\sigma_s^{\text{AH}})_{zx}$  is

$$t_{zx} \equiv -e^3 \chi v_0 \mathcal{G}_s B \epsilon_{zxy} \int \frac{d^3\mathbf{k}}{(2\pi)^3} (\Omega_s)^y \frac{k_x}{k^2} f'_0(\varepsilon_s) = 0. \quad (\text{C4})$$

Invoking the rotation symmetry of the dispersion about the  $k_x k_y$ -plane, we infer that, for  $\hat{\mathbf{e}}_E = \hat{\mathbf{y}}$ , we have  $t_{xy} = t_{zy} = 0$ . Next, let us assume that  $\hat{\mathbf{e}}_E = \hat{\mathbf{z}}$ , which involves setting  $\zeta_s = e \chi v_0 \mathcal{G}_s k_z B/k^2$ . The corresponding contribution to

1.  $(\sigma_s^{\text{AH}})_{xz}$  is

$$t_{xz} \equiv -e^3 \chi v_0 \mathcal{G}_s B \epsilon_{xzy} \int \frac{d^3\mathbf{k}}{(2\pi)^3} (\Omega_s)^y \frac{k_z}{k^2} f'_0(\varepsilon_s) = 0; \quad (\text{C5})$$

2.  $(\sigma_s^{\text{AH}})_{yz}$  is

$$t_{yz} \equiv -e^3 \chi v_0 \mathcal{G}_s B \epsilon_{yzx} \int \frac{d^3\mathbf{k}}{(2\pi)^3} (\Omega_s)^x \frac{k_z}{k^2} f'_0(\varepsilon_s) = 0. \quad (\text{C6})$$

## 2. Lorentz-force contribution

The leading-order contribution from the Lorentz-force part is obtained by picking up the  $n = 1$  term in the expression for  $g_s$  [shown in Eq. (34)], i.e., by using

$$\delta f_s^X(\mathbf{k}) = e^2 \tau^2 \mathcal{D}_s f'_0(\xi_s) \hat{L} [\mathcal{D}_s (\mathbf{w}_s + \mathbf{W}_s) \cdot \mathbf{E}]. \quad (\text{C7})$$

This leads to the conductivity [36]

$$\begin{aligned} (\sigma_s^{\text{LF}})_{ab} &= -\epsilon_{bdc} e^3 \tau^2 s^3 v_0^3 \int \frac{d^3 \mathbf{k}}{(2\pi)^3} \frac{\mathcal{D}_s^2}{\epsilon_s^5} [(w_s)_a + (W_s)_a] (\epsilon_s^2 - \lambda_s)^2 \frac{B_c k_d f'_0(\xi_s)}{k}, \\ \lambda_s &= 2 \chi e s \mathcal{G}_s v_0^2 \sum_{a'} \varrho_{a'} B_{a'}, \quad \boldsymbol{\varrho} = \cos \phi \sin \theta \hat{\mathbf{x}} + \sin \phi \sin \theta \hat{\mathbf{y}} + \cos \theta \hat{\mathbf{z}}, \end{aligned} \quad (\text{C8})$$

where  $\theta$  and  $\phi$  refer to the polar and azimuthal angles used in the spherical polar coordinate transformation in Eq. (B2). Using the same arguments as for the intrinsic anomalous-Hall part, we find that all the linear-in- $B$  components of  $(\sigma_s^{\text{LF}})_{ab}$  vanish.

## 3. Non-anomalous-Hall contribution

The non-anomalous-Hall part of the current is given by [cf. Eq. (A11)]

$$\bar{\mathbf{J}}_s = -e^2 \tau \int \frac{d^3 \mathbf{k}}{(2\pi)^3} [(\mathbf{w}_s + \mathbf{W}_s) \mathbf{B}] \mathcal{D}_s [(\mathbf{w}_s + \mathbf{W}_s) \cdot \mathbf{E}] f'_0(\xi_s), \quad (\text{C9})$$

leading to

$$(\bar{\sigma}_s)_{ab} = -e^2 \tau \int \frac{d^3 \mathbf{k}}{(2\pi)^3} \mathcal{D}_s [(w_s)_a + (W_s)_a] [(w_s)_b + (W_s)_b] f'_0(\xi_s). \quad (\text{C10})$$

We want to compute here the linear-in- $B$  part of  $\bar{\sigma}_s$ , after dividing it up as  $\sigma_s^{\text{BC}} + \sigma_s^m$ , where  $\sigma_s^{\text{BC}}$  arises solely due to the effect of the BC and survives when OMM is set to zero, and  $\sigma_s^m$  is the one which goes to zero if OMM is ignored.

### a. BC-only part (no OMM)

The BC-only part is given by

$$(\sigma_s^{\text{BC}})_{ab} = -\frac{e^3 \tau}{(2\pi)^3} \int d^3 \mathbf{k} \mathcal{M}_{ab} f'_0(\xi_s), \quad \mathcal{M}_{ab} = \left[ -\frac{(v_s)_a (v_s)_b}{2} (\boldsymbol{\Omega}_s \cdot \mathbf{B}) + (v_s)_a (\mathbf{v}_s \cdot \boldsymbol{\Omega}_s) B_b \right] + a \leftrightarrow b. \quad (\text{C11})$$

### b. Part with the integrand proportional to nonzero powers of OMM

In order to actually carry out the integration for this part, it is convenient to express  $\mathbf{u}_s$  as

$$(u_s)_a = \sum_b (\mathcal{U}_s)_{ab} B_b, \quad \mathcal{U}_s = \begin{bmatrix} \Delta_{11} & \Delta_{12} & \Delta_{13} \\ \Delta_{21} & \Delta_{22} & \Delta_{23} \\ \Delta_{31} & \Delta_{32} & \Delta_{33} \end{bmatrix}, \quad (\text{C12})$$

where

$$\begin{aligned} \Delta_{11}(\tilde{\epsilon}, \theta, \phi) &= -\chi e \mathcal{G}_s s^2 v_0^3 \frac{\sin^2 \theta \cos(2\phi) - \cos^2 \theta}{\tilde{\epsilon}^2}, & \Delta_{22}(\tilde{\epsilon}, \theta, \phi) &= \Delta_{11}(\tilde{\epsilon}, \theta, \frac{\pi}{2} - \phi), \\ \Delta_{33}(\tilde{\epsilon}, \theta, \phi) &= -\Delta_{11}(\tilde{\epsilon}, \theta, 0), & \Delta_{12}(\tilde{\epsilon}, \theta, \phi) &= \Delta_{21}(\tilde{\epsilon}, \theta, \phi) = -\chi e \mathcal{G}_s s^2 v_0^3 \frac{\sin^2 \theta \sin(2\phi)}{\tilde{\epsilon}^2}, \\ \Delta_{13}(\tilde{\epsilon}, \theta, \phi) &= \Delta_{31}(\tilde{\epsilon}, \theta, \phi) = \frac{\Delta_{12}}{\tan \theta \sin \phi}, & \Delta_{23}(\tilde{\epsilon}, \theta, \phi) &= \Delta_{32}(\tilde{\epsilon}, \theta, \phi) = \frac{\Delta_{12}}{\tan \theta \cos \phi}. \end{aligned} \quad (\text{C13})$$

We can now express the relevant part of conductivity as

$$\begin{aligned} (\sigma_s^m)_{ab} &= -e^2 \tau \int \frac{d^3 \mathbf{k}}{(2\pi)^3} [\mathcal{S}_{ab} f'_0(\xi_s) + \mathcal{P}_{ab} f''_0(\xi_s)], \\ \mathcal{S}_{ab} &= \left[ (v_s)_a \sum_c (\mathcal{U}_s)_{bc} B^c \right] + a \leftrightarrow b, \quad \mathcal{P}_{ab} = \left[ -\frac{(v_s)_a (v_s)_b}{2} (\mathbf{m}_s \cdot \mathbf{B}) \right] + a \leftrightarrow b. \end{aligned} \quad (\text{C14})$$

#### 4. Final expressions

Expressing the linear-in- $B$  part of the current and the conductivity as  $J_a^{\text{lin},s} = (\sigma_s^{\text{lin}})_{ab} E^b$  and  $(\sigma_s^{\text{lin}})_{ab}$ , respectively, let us define a third-rank tensor

$$(\zeta_s^{\text{lin}})^c{}_{ab} = \frac{\partial (\sigma_s^{\text{lin}})_{ab}}{\partial B_c}. \quad (\text{C15})$$

For our scenario with  $\mathbf{E} \parallel \mathbf{B}$ , we will be dealing with the vector defined as

$$\zeta_a^s = \sum_{b,c} (\zeta_s^{\text{lin}})^c{}_{ab} \delta^b{}_c = \sum_b (\zeta_s^{\text{lin}})^b{}_{ab}. \quad (\text{C16})$$

Gathering all the ingredients from the preceding subsections, we divide up  $\zeta_a^s$  as

$$\zeta_a^s = \zeta_a^{(s,1)} + \zeta_a^{(s,2)} + \zeta_a^{(s,3)} + \zeta_a^{(s,4)} + \zeta_a^{(s,5)}, \quad (\text{C17})$$

where

$$\begin{aligned} \zeta_a^{(s,1)} &= e^3 \tau \sum_b \int \frac{d^3 \mathbf{k}}{(2\pi)^3} (v_s)_a (v_s)^b (\Omega_s)_b f'_0(\varepsilon_s) = e^3 \tau \int \frac{d^3 \mathbf{k}}{(2\pi)^3} (v_s)_a (\mathbf{v}_s \cdot \boldsymbol{\Omega}_s) f'_0(\varepsilon_s), \\ \zeta_a^{(s,2)} &= -e^3 \tau \sum_b (1 + \delta_{ab}) \int \frac{d^3 \mathbf{k}}{(2\pi)^3} (v_s)_a (\mathbf{v}_s \cdot \boldsymbol{\Omega}_s) f'_0(\varepsilon_s) = -4 \zeta_a^{(s,1)}, \\ \zeta_a^{(s,3)} &= e^2 \tau \sum_b \int \frac{d^3 \mathbf{k}}{(2\pi)^3} (v_s)_a [\partial_{k_b} (m_s)_b] f'_0(\varepsilon_s) = \frac{e^3 \tau v_0 \mathcal{G}_s}{s} \int \frac{d^3 \mathbf{k}}{(2\pi)^3} (v_s)_a [\nabla_{\mathbf{k}} \cdot (k \boldsymbol{\Omega}_s)] f'_0(\varepsilon_s) \text{ [since } \mathbf{m}_s(\mathbf{k}) = \frac{e v_0 \mathcal{G}_s k}{s} \boldsymbol{\Omega}_s(\mathbf{k})], \\ \zeta_a^{(s,4)} &= e^2 \tau \sum_b \int \frac{d^3 \mathbf{k}}{(2\pi)^3} (v_s)^b [\partial_{k_a} (m_s)_b] f'_0(\varepsilon_s) = \frac{e^3 \tau v_0 \mathcal{G}_s}{s} \int \frac{d^3 \mathbf{k}}{(2\pi)^3} [\mathbf{v}_s \cdot \partial_{k_a} (k \boldsymbol{\Omega}_s)] f'_0(\varepsilon_s), \\ \zeta_a^{(s,5)} &= e^2 \tau \sum_b \int \frac{d^3 \mathbf{k}}{(2\pi)^3} (v_s)_a (v_s)^b (m_s)_b f''_0(\varepsilon_s) = \frac{e^3 \tau v_0 \mathcal{G}_s}{s} \int \frac{d^3 \mathbf{k}}{(2\pi)^3} (v_s)_a k (\mathbf{v}_s \cdot \boldsymbol{\Omega}_s) f''_0(\varepsilon_s). \end{aligned} \quad (\text{C18})$$

While  $\zeta_a^{(s,1)}$  and  $\zeta_a^{(s,2)}$  represent the parts arising purely from the BC (i.e., with no contribution from the OMM),  $\zeta_a^{(s,3)}$ ,  $\zeta_a^{(s,4)}$ , and  $\zeta_a^{(s,5)}$  are the terms which go to zero if OMM is neglected.

Below, we elucidate the final expressions:

1. Noting that  $\mathbf{v}_s \cdot \boldsymbol{\Omega}_s = -\frac{\chi v_0 s}{k^2} (s + \eta \cos \theta)$ , and using Eq. (B5), we obtain

$$\zeta_a^{(s,1)} = -\delta_{za} \chi v_0 s e^3 \tau \int \frac{d^3 \mathbf{k}}{(2\pi)^3} (\eta + s \cos \theta) \frac{s + \eta \cos \theta}{k^2} f'_0(\varepsilon_s) = -\frac{\delta_{za} \eta v_0 e^3 \tau \mathcal{C}_s}{4\pi^2}. \quad (\text{C19})$$

2. Noting that  $\nabla_{\mathbf{k}} \cdot (k \boldsymbol{\Omega}_s) = -\chi s/k^2$ , and using Eq. (B5), we obtain

$$\begin{aligned} \zeta_a^{(s,3)} &= -\frac{\delta_{za} \chi e^3 \tau v_0^2 \mathcal{G}_s}{(2\pi)^3} \int d^3 \mathbf{k} \frac{\eta + s \cos \theta}{k^2} f'_0(\varepsilon_s) \\ &= -\frac{\delta_{za} \chi e^3 \tau v_0^2 \mathcal{G}_s}{(2\pi)^2} \int d\theta \int d\tilde{\varepsilon} \frac{\tilde{\varepsilon}^2 \sin \theta}{s^3 v_0^3} \frac{\eta + s \cos \theta}{k^2} \frac{s f'_0(\tilde{\varepsilon})}{s + \eta \cos \theta} \\ &= -\frac{\delta_{za} \chi v_0 e^3 \tau \mathcal{G}_s}{2\pi^2} \frac{(s^2 - \eta^2) \tanh^{-1}(\frac{\eta}{s}) - \eta s}{\eta^2} \text{ for } |\eta| < |s|. \end{aligned} \quad (\text{C20})$$

3. Noting that  $\mathbf{v}_s \cdot \partial_{k_a} (k \boldsymbol{\Omega}_s) = -\chi s (v_s)_a / k^2$ , we obtain

$$\zeta_a^{(s,4)} = -\frac{\delta_{za} \chi s e^3 \tau v_0 \mathcal{G}_s}{s} \int \frac{d^3 \mathbf{k}}{(2\pi)^3} \frac{(v_s)_z}{k^2} f'_0(\varepsilon_s) = \zeta_a^{(s,3)}. \quad (\text{C21})$$

4. Noting that  $\mathbf{v}_s \cdot \boldsymbol{\Omega}_s = -\frac{\chi v_0 s}{k^2} (s + \eta \cos \theta)$ , we obtain

$$\zeta_a^{(s,5)} = -\delta_{za} \chi e^3 \tau v_0^3 \mathcal{G}_s \int \frac{d^3 \mathbf{k}}{(2\pi)^3} (\eta + s \cos \theta) \frac{s + \eta \cos \theta}{k} f''_0(\varepsilon_s) = -\zeta_a^{(s,3)}. \quad (\text{C22})$$



- 
- [1] A. A. Burkov and L. Balents, Weyl semimetal in a topological insulator multilayer, *Phys. Rev. Lett.* **107**, 127205 (2011).
- [2] B. Yan and C. Felser, Topological materials: Weyl semimetals, *Annual Rev. of Condensed Matter Phys.* **8**, 337 (2017).
- [3] N. P. Armitage, E. J. Mele, and A. Vishwanath, Weyl and Dirac semimetals in three-dimensional solids, *Rev. Mod. Phys.* **90**, 015001 (2018).
- [4] M. M. H. Polash, S. Yalameha, H. Zhou, K. Ahadi, Z. Nourbakhsh, and D. Vashaee, Topological quantum matter to topological phase conversion: Fundamentals, materials, physical systems for phase conversions, and device applications, *Materials Science and Engineering: R: Reports* **145**, 100620 (2021).
- [5] S. Sekh and I. Mandal, Circular dichroism as a probe for topology in three-dimensional semimetals, *Phys. Rev. B* **105**, 235403 (2022).
- [6] I. Mandal, Signatures of two- and three-dimensional semimetals from circular dichroism, *International Journal of Modern Physics B* **38**, 2450216 (2024).
- [7] J. E. Moore, Optical properties of Weyl semimetals, *National Science Rev.* **6**, 206 (2018).
- [8] C. Guo, V. S. Asadchy, B. Zhao, and S. Fan, Light control with Weyl semimetals, *eLight* **3**, 2 (2023).
- [9] A. Avdoshkin, V. Kozii, and J. E. Moore, Interactions remove the quantization of the chiral photocurrent at Weyl points, *Phys. Rev. Lett.* **124**, 196603 (2020).
- [10] I. Mandal, Effect of interactions on the quantization of the chiral photocurrent for double-Weyl semimetals, *Symmetry* **12** (2020).
- [11] M. Papaj and L. Fu, Magnus Hall effect, *Phys. Rev. Lett.* **123**, 216802 (2019).
- [12] D. Mandal, K. Das, and A. Agarwal, Magnus Nernst and thermal Hall effect, *Phys. Rev. B* **102**, 205414 (2020).
- [13] Sekh, Sajid and Mandal, Ipsita, Magnus Hall effect in three-dimensional topological semimetals, *Eur. Phys. J. Plus* **137**, 736 (2022).
- [14] F. D. M. Haldane, Berry curvature on the Fermi surface: Anomalous Hall effect as a topological Fermi-liquid property, *Phys. Rev. Lett.* **93**, 206602 (2004).
- [15] P. Goswami and S. Tewari, Axionic field theory of (3 + 1)-dimensional Weyl semimetals, *Phys. Rev. B* **88**, 245107 (2013).
- [16] A. A. Burkov, Anomalous Hall effect in Weyl metals, *Phys. Rev. Lett.* **113**, 187202 (2014).
- [17] S.-B. Zhang, H.-Z. Lu, and S.-Q. Shen, Linear magnetoconductivity in an intrinsic topological Weyl semimetal, *New Journal of Phys.* **18**, 053039 (2016).
- [18] Q. Chen and G. A. Fiete, Thermoelectric transport in double-Weyl semimetals, *Phys. Rev. B* **93**, 155125 (2016).
- [19] S. Nandy, G. Sharma, A. Taraphder, and S. Tewari, Chiral anomaly as the origin of the planar Hall effect in Weyl semimetals, *Phys. Rev. Lett.* **119**, 176804 (2017).
- [20] S. Nandy, A. Taraphder, and S. Tewari, Berry phase theory of planar Hall effect in topological insulators, *Scientific Reports* **8**, 14983 (2018).
- [21] K. Das and A. Agarwal, Linear magnetochiral transport in tilted type-I and type-II Weyl semimetals, *Phys. Rev. B* **99**, 085405 (2019).
- [22] K. Das and A. Agarwal, Thermal and gravitational chiral anomaly induced magneto-transport in Weyl semimetals, *Phys. Rev. Res.* **2**, 013088 (2020).
- [23] S. Das, K. Das, and A. Agarwal, Nonlinear magnetoconductivity in Weyl and multi-Weyl semimetals in quantizing magnetic field, *Phys. Rev. B* **105**, 235408 (2022).
- [24] O. Pal, B. Dey, and T. K. Ghosh, Berry curvature induced magnetotransport in 3D noncentrosymmetric metals, *Journal of Phys.: Condensed Matter* **34**, 025702 (2022).
- [25] O. Pal, B. Dey, and T. K. Ghosh, Berry curvature induced anisotropic magnetotransport in a quadratic triple-component fermionic system, *Journal of Phys.: Condensed Matter* **34**, 155702 (2022).
- [26] L. X. Fu and C. M. Wang, Thermoelectric transport of multi-Weyl semimetals in the quantum limit, *Phys. Rev. B* **105**, 035201 (2022).
- [27] Y. Araki, Magnetic Textures and Dynamics in Magnetic Weyl Semimetals, *Annalen der Physik* **532**, 1900287 (2020).
- [28] Y. P. Mizuta and F. Ishii, Contribution of Berry curvature to thermoelectric effects, *Proceedings of the International Conference on Strongly Correlated Electron Systems (SCES2013)*, *JPS Conf. Proc.* **3**, 017035 (2014).
- [29] S. Yadav, S. Fazzini, and I. Mandal, Magneto-transport signatures in periodically-driven Weyl and multi-Weyl semimetals, *Physica E Low-Dimensional Systems and Nanostructures* **144**, 115444 (2022).
- [30] A. Knoll, C. Timm, and T. Meng, Negative longitudinal magnetoconductance at weak fields in Weyl semimetals, *Phys. Rev. B* **101**, 201402 (2020).
- [31] L. Medel Onofre and A. Martín-Ruiz, Planar Hall effect in Weyl semimetals induced by pseudoelectromagnetic fields, *Phys. Rev. B* **108**, 155132 (2023).
- [32] R. Ghosh and I. Mandal, Electric and thermoelectric response for Weyl and multi-Weyl semimetals in planar Hall configurations including the effects of strain, *Physica E: Low-dimensional Systems and Nanostructures* **159**, 115914 (2024).
- [33] R. Ghosh and I. Mandal, Direction-dependent conductivity in planar Hall set-ups with tilted Weyl/multi-Weyl semimetals, *Journal of Physics: Condensed Matter* **36**, 275501 (2024).
- [34] I. Mandal and K. Saha, Thermoelectric response in nodal-point semimetals, *Ann. Phys. (Berlin)* (**Early View version**), 202400016 (2024), arXiv:2309.10763 [cond-mat.mes-hall].
- [35] L. Medel, R. Ghosh, A. Martín-Ruiz, and I. Mandal, Electric, thermal, and thermoelectric magnetoconductivity for Weyl/multi-Weyl semimetals in planar Hall set-ups induced by the combined effects of topology and strain, *Scientific Reports* **14**, 21390 (2024).
- [36] R. Ghosh, F. Haidar, and I. Mandal, Linear response in planar Hall and thermal Hall setups for Rarita-Schwinger-Weyl semimetals, arXiv e-prints (2024), arXiv:2408.01422 [cond-mat.mes-hall].

- [37] V. Gusynin, S. Sharapov, and J. Carbotte, Magneto-optical conductivity in graphene, *Journal of Phys.: Condensed Matter* **19**, 026222 (2006).
- [38] M. Stålhammar, J. Larana-Aragon, J. Knolle, and E. J. Bergholtz, Magneto-optical conductivity in generic Weyl semimetals, *Phys. Rev. B* **102**, 235134 (2020).
- [39] S. Yadav, S. Sekh, and I. Mandal, Magneto-optical conductivity in the type-I and type-II phases of Weyl/multi-Weyl semimetals, *Physica B: Condensed Matter* **656**, 414765 (2023).
- [40] I. Mandal and A. Sen, Tunneling of multi-Weyl semimetals through a potential barrier under the influence of magnetic fields, *Phys. Lett. A* **399**, 127293 (2021).
- [41] S. Bera and I. Mandal, Floquet scattering of quadratic band-touching semimetals through a time-periodic potential well, *Journal of Phys. Condensed Matter* **33**, 295502 (2021).
- [42] S. Bera, S. Sekh, and I. Mandal, Floquet transmission in Weyl/multi-Weyl and nodal-line semimetals through a time-periodic potential well, *Ann. Phys. (Berlin)* **535**, 2200460 (2023).
- [43] D. Sinha and K. Sengupta, Transport across junctions of a weyl and a multi-weyl semimetal, *Phys. Rev. B* **99**, 075153 (2019).
- [44] I. Mandal, Transmission and conductance across junctions of isotropic and anisotropic three-dimensional semimetals, *European Physical Journal Plus* **138**, 1039 (2023).
- [45] B. Bradlyn, J. Cano, Z. Wang, M. G. Vergniory, C. Felser, R. J. Cava, and B. A. Bernevig, Beyond Dirac and Weyl fermions: Unconventional quasiparticles in conventional crystals, *Science* **353** (2016).
- [46] L. Liang and Y. Yu, Semimetal with both Rarita-Schwinger-Weyl and Weyl excitations, *Phys. Rev. B* **93**, 045113 (2016).
- [47] I. Boettcher, Interplay of topology and electron-electron interactions in Rarita-Schwinger-Weyl semimetals, *Phys. Rev. Lett.* **124**, 127602 (2020).
- [48] J. M. Link, I. Boettcher, and I. F. Herbut,  $d$ -wave superconductivity and Bogoliubov-Fermi surfaces in Rarita-Schwinger-Weyl semimetals, *Phys. Rev. B* **101**, 184503 (2020).
- [49] H. Isobe and L. Fu, Quantum critical points of  $j = \frac{3}{2}$  Dirac electrons in antiperovskite topological crystalline insulators, *Phys. Rev. B* **93**, 241113 (2016).
- [50] P. Tang, Q. Zhou, and S.-C. Zhang, Multiple types of topological fermions in transition metal silicides, *Phys. Rev. Lett.* **119**, 206402 (2017).
- [51] I. Mandal, Transmission in pseudospin-1 and pseudospin-3/2 semimetals with linear dispersion through scalar and vector potential barriers, *Physics Letters A* **384**, 126666 (2020).
- [52] J.-Z. Ma, Q.-S. Wu, M. Song, S.-N. Zhang, E. Guedes, S. Ekahana, M. Krivenkov, M. Yao, S.-Y. Gao, W.-H. Fan, *et al.*, Observation of a singular Weyl point surrounded by charged nodal walls in ptga, *Nature Communications* **12**, 3994 (2021).
- [53] I. Mandal, Andreev bound states in superconductor-barrier-superconductor junctions of Rarita-Schwinger-Weyl semimetals, *Physics Letters A* **503**, 129410 (2024).
- [54] S. Weinberg, *The quantum theory of fields. Vol. 3: Supersymmetry* (Cambridge University Press, 2013).
- [55] J. Cayssol and J. N. Fuchs, Topological and geometrical aspects of band theory, *Journal of Physics: Materials* **4**, 034007 (2021).
- [56] H. Nielsen and M. Ninomiya, A no-go theorem for regularizing chiral fermions, *Phys. Lett. B* **105**, 219 (1981).
- [57] D. Takane, Z. Wang, S. Souma, K. Nakayama, T. Nakamura, H. Oinuma, Y. Nakata, H. Iwasawa, C. Cacho, T. Kim, K. Horiba, H. Kumigashira, T. Takahashi, Y. Ando, and T. Sato, Observation of chiral fermions with a large topological charge and associated fermi-arc surface states in *cosi*, *Phys. Rev. Lett.* **122**, 076402 (2019).
- [58] D. S. Sanchez, I. Belopolski, T. A. Cochran, X. Xu, J.-X. Yin, G. Chang, W. Xie, K. Manna, V. Süß, C.-Y. Huang, *et al.*, Topological chiral crystals with helicoid-arc quantum states, *Nature* **567**, 500 (2019).
- [59] N. B. Schröter, D. Pei, M. G. Vergniory, Y. Sun, K. Manna, F. De Juan, J. A. Krieger, V. Süß, M. Schmidt, P. Dudin, *et al.*, Chiral topological semimetal with multifold band crossings and long fermi arcs, *Nature Physics* **15**, 759 (2019).
- [60] B. Q. Lv, Z.-L. Feng, J.-Z. Zhao, N. F. Q. Yuan, A. Zong, K. F. Luo, R. Yu, Y.-B. Huang, V. N. Strocov, A. Chikina, A. A. Soluyanov, N. Gedik, Y.-G. Shi, T. Qian, and H. Ding, Observation of multiple types of topological fermions in *pdbise*, *Phys. Rev. B* **99**, 241104 (2019).
- [61] R. Flores-Calderón and A. Martín-Ruiz, Quantized electrochemical transport in Weyl semimetals, *Phys. Rev. B* **103**, 035102 (2021).
- [62] F. Balduini, A. Molinari, L. Rocchino, V. Hasse, C. Felser, M. Sousa, C. Zota, H. Schmid, A. G. Grushin, and B. Gotsmann, Intrinsic negative magnetoresistance from the chiral anomaly of multifold fermions, *Nature Communications* **15**, 6526 (2024).
- [63] F. Flicker, F. de Juan, B. Bradlyn, T. Morimoto, M. G. Vergniory, and A. G. Grushin, Chiral optical response of multifold fermions, *Phys. Rev. B* **98**, 155145 (2018).
- [64] Y. Shen, Y. Jin, Y. Ge, M. Chen, and Z. Zhu, Chiral topological metals with multiple types of quasiparticle fermions and large spin Hall effect in the SrGePt family materials, *Phys. Rev. B* **108**, 035428 (2023).
- [65] G. Chang, S.-Y. Xu, B. J. Wieder, D. S. Sanchez, S.-M. Huang, I. Belopolski, T.-R. Chang, S. Zhang, A. Bansil, H. Lin, and M. Z. Hasan, Unconventional chiral fermions and large topological Fermi arcs in RhSi, *Phys. Rev. Lett.* **119**, 206401 (2017).
- [66] K. Nakazawa, T. Yamaguchi, and A. Yamakage, Nonlinear charge and thermal transport properties induced by orbital magnetic moment in chiral crystal cobalt monosilicide, arXiv e-prints (2024), [arXiv:2409.08040 \[cond-mat.str-el\]](https://arxiv.org/abs/2409.08040).
- [67] D. Xiao, M.-C. Chang, and Q. Niu, Berry phase effects on electronic properties, *Rev. Mod. Phys.* **82**, 1959 (2010).
- [68] N. Ashcroft and N. Mermin, *Solid State Physics* (Cengage Learning, 2011).
- [69] C. Zeng, S. Nandy, and S. Tewari, Fundamental relations for anomalous thermoelectric transport coefficients in the nonlinear regime, *Phys. Rev. Res.* **2**, 032066 (2020).
- [70] L. Onsager, Reciprocal Relations in Irreversible Processes. I., *Phys. Rev.* **37**, 405 (1931).
- [71] H. B. G. Casimir, On Onsager's principle of microscopic reversibility, *Rev. Mod. Phys.* **17**, 343 (1945).
- [72] P. Jacquod, R. S. Whitney, J. Meair, and M. Büttiker, Onsager relations in coupled electric, thermoelectric, and spin transport: The tenfold way, *Phys. Rev. B* **86**, 155118 (2012).
- [73] L. Li, C. Cui, R.-W. Zhang, Z.-M. Yu, and Y. Yao, Planar Hall plateau in magnetic Weyl semimetals, arXiv e-prints (2024), [arXiv:2406.11273 \[cond-mat.mes-hall\]](https://arxiv.org/abs/2406.11273).

- [74] I. Mandal and K. Saha, Thermopower in an anisotropic two-dimensional Weyl semimetal, *Phys. Rev. B* **101**, 045101 (2020).
- [75] J. Xiong, S. Kushwaha, J. Krizan, T. Liang, R. J. Cava, and N. P. Ong, Anomalous conductivity tensor in the Dirac semimetal  $\text{Na}_3\text{Bi}$ , *EPL (Europhysics Letters)* **114**, 27002 (2016).
- [76] G. Sundaram and Q. Niu, Wave-packet dynamics in slowly perturbed crystals: Gradient corrections and Berry-phase effects, *Phys. Rev. B* **59**, 14915 (1999).
- [77] L. Li, J. Cao, C. Cui, Z.-M. Yu, and Y. Yao, Planar Hall effect in topological Weyl and nodal-line semimetals, *Phys. Rev. B* **108**, 085120 (2023).
- [78] D. T. Son and B. Z. Spivak, Chiral anomaly and classical negative magnetoresistance of Weyl metals, *Phys. Rev. B* **88**, 104412 (2013).
- [79] D. Xiao, J. Shi, and Q. Niu, Berry Phase Correction to Electron Density of States in Solids, *Phys. Rev. Lett.* **95**, 137204 (2005).
- [80] C. Duval, Z. Horváth, P. A. Horvathy, L. Martina, and P. Stichel, Berry phase correction to electron density in solids and “exotic” dynamics, *Mod. Phys. Lett. B* **20**, 373 (2006).
- [81] D. T. Son and N. Yamamoto, Berry curvature, triangle anomalies, and the chiral magnetic effect in Fermi liquids, *Phys. Rev. Lett.* **109**, 181602 (2012).
- [82] R. Lundgren, P. Laurell, and G. A. Fiete, Thermoelectric properties of Weyl and Dirac semimetals, *Phys. Rev. B* **90**, 165115 (2014).
- [83] D. Xiao, Y. Yao, Z. Fang, and Q. Niu, Berry-phase effect in anomalous thermoelectric transport, *Phys. Rev. Lett.* **97**, 026603 (2006).
- [84] K. Das and A. Agarwal, Berry curvature induced thermopower in type-I and type-II Weyl semimetals, *Phys. Rev. B* **100**, 085406 (2019).
- [85] N. R. Cooper, B. I. Halperin, and I. M. Ruzin, Thermoelectric response of an interacting two-dimensional electron gas in a quantizing magnetic field, *Phys. Rev. B* **55**, 2344 (1997).
- [86] E. W. Weisstein, Regularized hypergeometric function, *From MathWorld—A Wolfram Web Resource* (Wolfram Research, Inc.).